FIELD AND LABORATORY STUDY OF HIGH-POLYMER MIXTURES AT THE NCAT TEST TRACK: FINAL REPORT

By
Dr. David H. Timm
Dr. Mary M. Robbins
Dr. J. Richard Willis
Dr. Nam Tran
Adam J. Taylor

February 20, 2013

National Center for Asphalt Technology

NCAT

at AUBURN UNIVERSITY

277 Technology Parkway ▪ Auburn, AL 36830

NCAT Report 13-03

**Field and Laboratory Study of High-Polymer Mixtures at the NCAT Test Track:
Final Report**

By
Dr. David H. Timm
Dr. Mary M. Robbins
Dr. J. Richard Willis
Dr. Nam Tran
Adam J. Taylor

National Center for Asphalt Technology
Auburn University

February 20, 2013

DISCLAIMER

The contents of this report reflect the views of the authors who are responsible for the facts and accuracy of the data presented herein. The contents do not necessarily reflect the official views or policies of Kraton Performance Polymers, Inc. or the National Center for Asphalt Technology, or Auburn University. This report does not constitute a standard, specification, or regulation. Comments contained in this paper related to specific testing equipment and materials should not be considered an endorsement of any commercial product or service; no such endorsement is intended or implied.

TABLE OF CONTENTS

LIST OF TABLES

LIST OF FIGURES

1. INTRODUCTION

1.1 Background

In 2009, Kraton Performance Polymers, Inc. began sponsorship of a full-scale test section at the National Center for Asphalt Technology (NCAT) Test Track featuring their newly developed highly polymer modified (HPM) asphalt. The HPM mixtures were designed with 7.5% styrene-butadiene-styrene (SBS) polymer to have much improved fatigue and rutting resistance characteristics over conventional materials. As documented in an earlier report (Timm et al., 2012), four-point bending beam fatigue testing on mixtures with these binders has shown well over an order of magnitude increase in fatigue life (van de Ven et al., 2007; Molenaar et al., 2008; Kluttz et al., 2009). Additionally, 3D finite element modeling using the continuum damage Asphalt Concrete Response (ACRe) model developed by TU Delft (Scarpas and Blaauwendraad, 1998; Erkens, 2002) predicts improved resistance to permanent deformation and fatigue damage even with a 40% reduction in thickness (Halper and Holden, 1988; von Quintus, 2005; Anderson, 2007).

The Kraton section was built at the same time as a control section, using conventional materials, and opened to traffic as part of the 2009 Test Track research cycle. Figure 1.1 shows the structural designs for each section. The Kraton section was designed with 5.75 inches of asphalt concrete (AC) over 6 inches of granular base while the control section was designed with the same depth of aggregate base and 7 inches of AC.

	Kraton	Control
Agg Base	6	6
Lift3	2.25	3
Lift2	2.25	2.75
Lift1	1.25	1.25
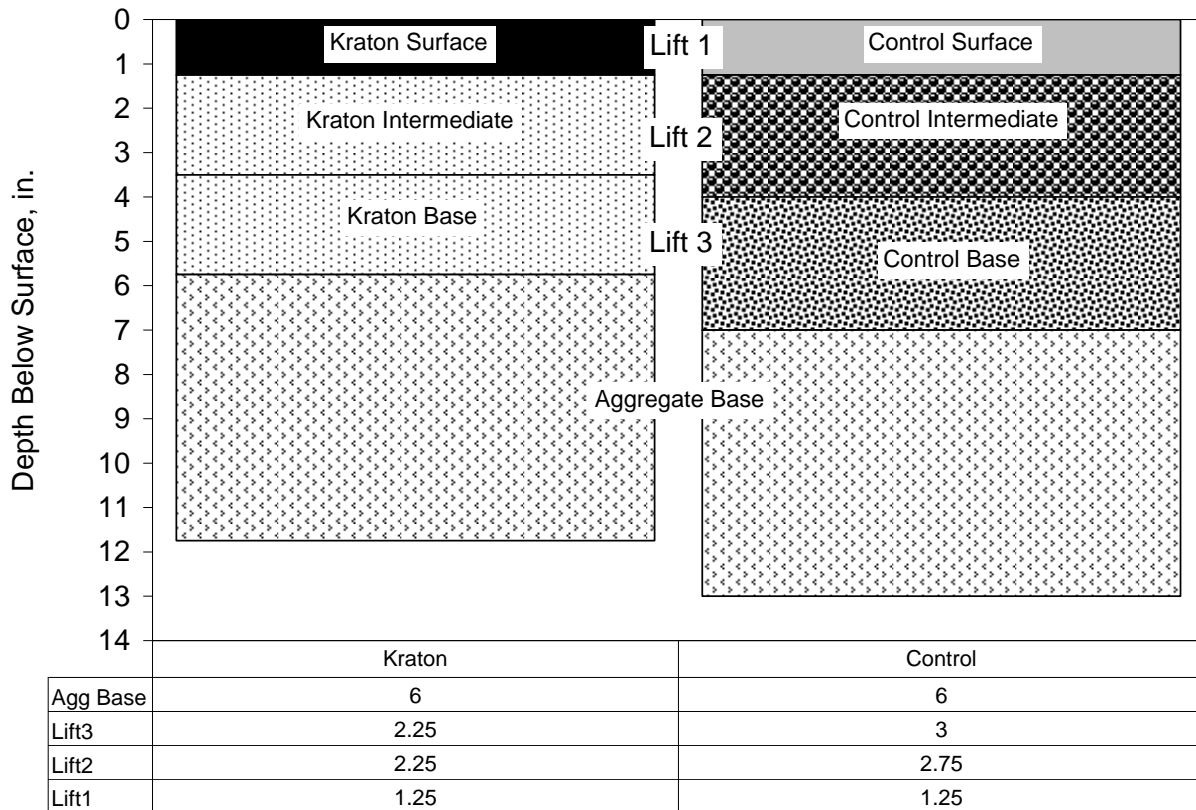
Figure 1.1 Cross-Section Design: Materials and Lift Thicknesses

The materials and mix design were previously documented (Timm et al., 2012) while only a summary is provided here. Two design gradations were used in this study. The surface layers utilized a 9.5 mm nominal maximum aggregate size (NMAS) while the intermediate and base mixtures used a 19 mm NMAS gradation. The aggregate gradations were a blend of granite, limestone and sand using locally available materials. Distinct gradations were developed for each control mixture (surface, intermediate and base) to achieve the necessary volumetric targets as the binder grade and nominal maximum aggregate size (NMAS) changed between layers. The Kraton gradations were very similar to the control mixtures. Table 1.1 provides a summary of the mix design parameters while further details are available in Appendix A and the previous report (Timm et al., 2012).

Table 1.1 Mix Design Parameters

Mixture Type	Control (S9)			Kraton (N7)	
Lift (1=surface; 2=intermediate, 3=base)	1	2	3	1	2 & 3
Asphalt PG Grade	76-22	76-22	67-22	88-22	88-22
% Polymer Modification	2.8	2.8	0	7.5	7.5
Design Air Voids (VTM), %	4	4	4	4	4
Total Combined Binder (P_b), % wt	5.8	4.7	4.6	5.9	4.6
Effective Binder (P_{be}), %	5.1	4.1	4.1	5.3	4.2
Dust Proportion (DP)	1.1	0.9	1.1	1.1	0.9
Maximum Specific Gravity (G_{mm})	2.483	2.575	2.574	2.474	2.570
Voids in Mineral Aggregate (VMA), %	15.8	13.9	13.9	16.2	14.0
Voids Filled with Asphalt (VFA), %	75	71	71	75	72

During construction, sensors were embedded in each section to measure horizontal strain at the bottom of the AC, vertical pressure at the top of the aggregate base, vertical pressure at the top of the subgrade and temperatures at various depths throughout the cross-section (Figure 1.2). The strain and pressure measurements were made on a weekly basis during the two-year test cycle while the temperature measurements were made minute-by-minute from which hourly averages were determined. Extensive falling weight deflectometer (FWD) testing was conducted at twelve random locations throughout the test section, as noted in Figure 1.3, several times per month to document effects of pavement temperature, aging and potential pavement damage on backcalculated AC moduli during the two-year cycle. Full details regarding the instrumentation and FWD testing have been previously documented (Timm et al., 2012).
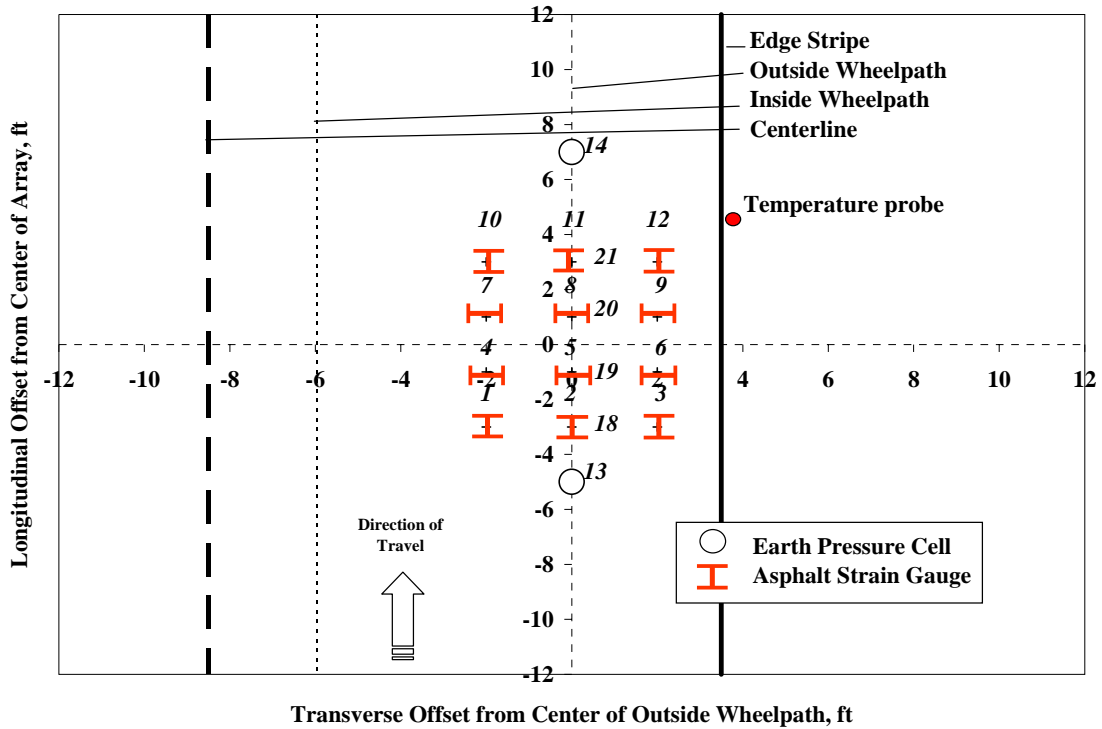
Figure 1.2 Gauge Array
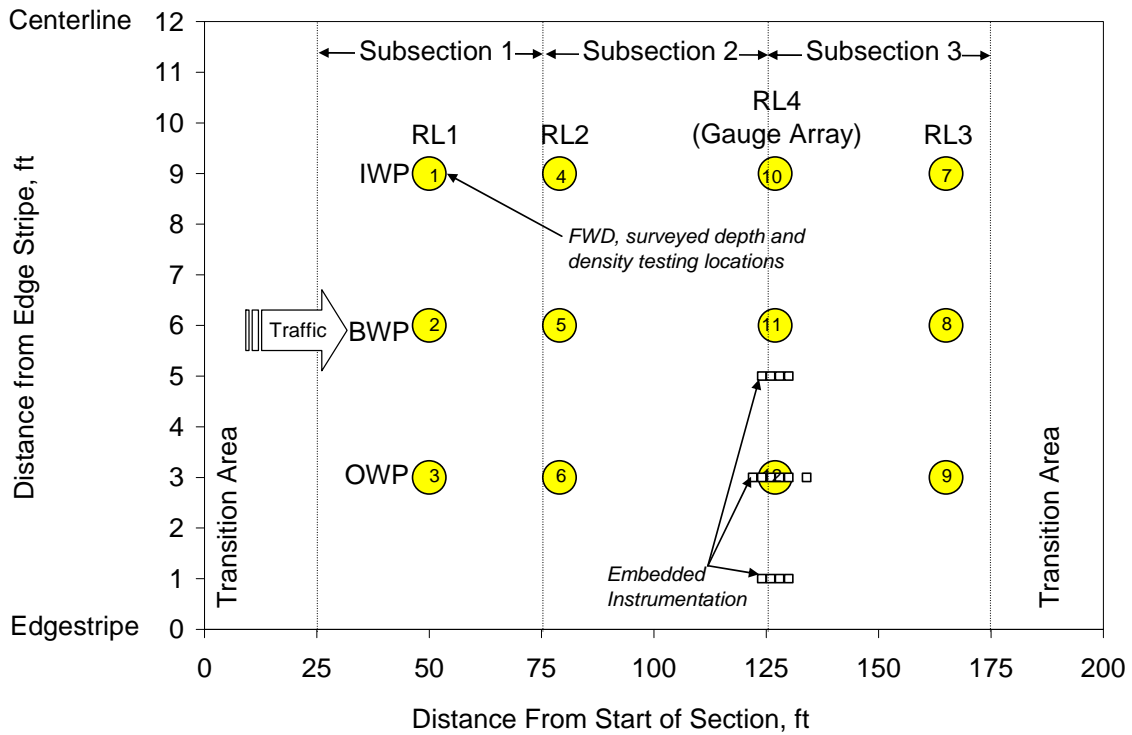
Figure 1.3 Random Locations and Instrumentation Schematic

At the time of construction, plant-produced mixtures were sampled for extensive laboratory testing. The previous, interim, report (Timm et al., 2012) documented the sampling, fabrication of specimens and results of the following tests:
- Binder performance grading
- Multiple stress creep recovery (MSCR)
- Dynamic modulus ($|E^*|$)
- Bending beam fatigue
- Asphalt pavement analyzer (APA)
- Flow Number (F_n)
- Indirect Tension (IDT) Creep Compliance and Strength
- Energy Ratio
- Moisture Susceptibility

Since the completion of the report, the following tests have been completed and are documented in this report:
- *Simplified Viscoelastic Continuum Damage (S-VECD) Fatigue Testing*
- *Hamburg Wheel Tracking Test (HWTT)*

The sections were opened to traffic on August 28, 2009. At that time, weekly pavement response and regular FWD testing began. Weekly performance monitoring, in terms of rutting, ride quality, and visual inspection for cracking, also commenced at that time. Trafficking ended on September 28, 2011 after the application of 10.14 million equivalent single axle loads (ESALs).

1.2 Objectives and Scope of Work
As mentioned previously, an interim report documenting initial findings through June, 2011 (8.9 million ESAL) was previously published (Timm et al., 2012). The objective of this report is to document findings from the laboratory testing not previously published and to present the entire two-year pavement response and performance history. This report relies upon the earlier report (Timm et al., 2012) as a reference document.

2. LABORATORY TESTING ON BINDERS AND PLANT PRODUCED MIXTURES
As described in the previous report (Timm et al., 2012), samples of asphalt binder and plant-produced mix were obtained at the Test Track during construction for characterization in the laboratory. The previous report detailed the sampling process, specimen fabrication and presented results of the following tests:
- Binder performance grading
- Multiple stress creep recovery (MSCR)
- Dynamic modulus ($|E^*|$)
- Bending beam fatigue
- Asphalt pavement analyzer (APA)
- Flow Number (F_n)
- Indirect Tension (IDT) Creep Compliance and Strength
- Energy Ratio
- Moisture Susceptibility

Since the completion of the previous report (Timm et al., 2012), additional testing was conducted at the direction of the research sponsor. These tests included:
- S-VECD Fatigue Testing
- HWTT

The following subsections detail the additional testing.

2.1 S-VECD Results
While fatigue testing based on continuum damage mechanics has been studied and documented (Kim et al, 1997; Daniel and Kim, 2002; Hou et al., 2010; Underwood et al., 2006), Dr. Richard Kim at North Carolina State University has recently developed a uniaxial fatigue test that can be performed in an Asphalt Mixture Performance Tester (AMPT). In this test, the asphalt specimen is tested in a displacement-controlled mode. The uniaxial fatigue data, in conjunction with dynamic modulus data, are analyzed based on the Simplified Viscoelastic Continuum Damage (S-VECD) model to determine the fatigue resistance of the asphalt mixture. The complete methodology for this test procedure has been documented elsewhere (Kim et al., 2009). S-VECD testing was performed for the base layer mixtures—N7-3 mix for the Kraton section and S9-3 mix for the control section—as it has been assumed that fatigue cracking normally initiates at the bottom of the asphalt structure and propagates upwards.

One output of the S-VECD testing methodology is the pseudo-stiffness (C) versus damage parameter (S) curve. The C and S parameters represent the material's integrity and the level of damage as testing progresses, respectively. For each mixture, a single C versus S curve can be determined regardless of the applied loading conditions and testing temperatures (Daniel and Kim, 2002). The curves for both mixtures (Figure 2.1) were modeled using a power model and were generated in the fatigue analysis software Alpha Fatigue. Each curve was plotted to the average C at which the samples for the mixture failed. The C versus S curves were then analyzed with the |E*| of the mixtures to fully evaluate their fatigue resistance. Figure 2.2 shows the predicted cycles to failure for both mixtures at various strain levels as they would be determined using the beam fatigue testing protocol at 10 Hz and 20°C. As can be seen, at similar strain magnitudes, the Kraton mixture always was predicted to have a larger fatigue life than the control base mixture. These trends are in agreement with those previously seen for these mixtures using the beam fatigue test.
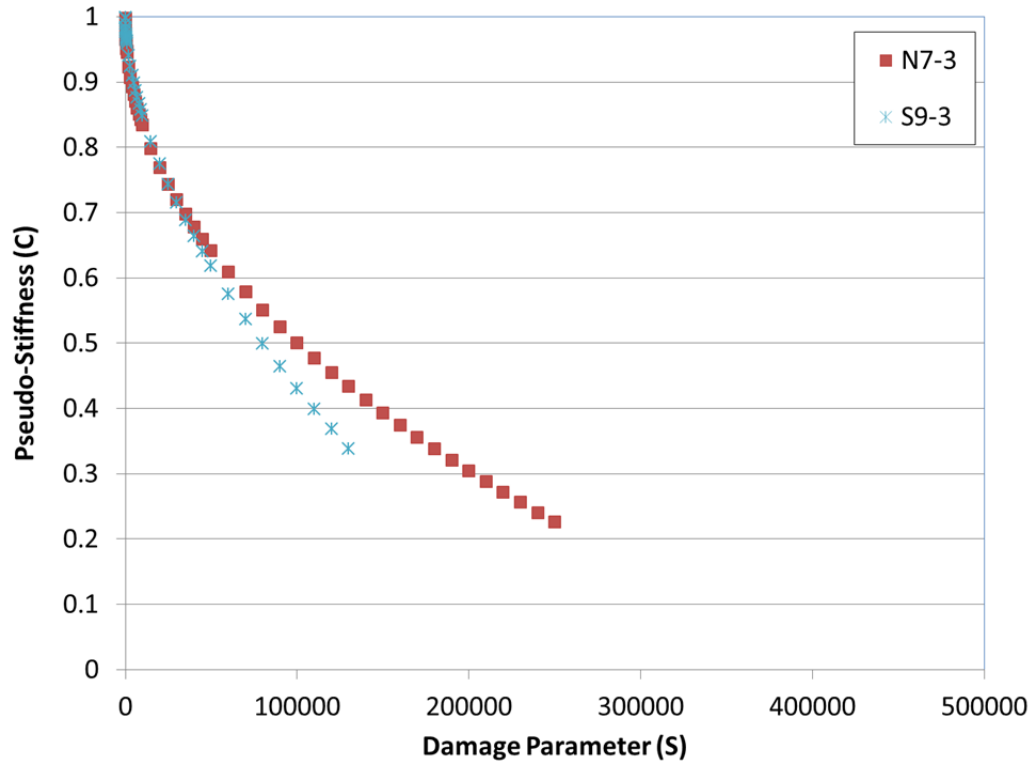
Figure 2.1 C vs. S curve
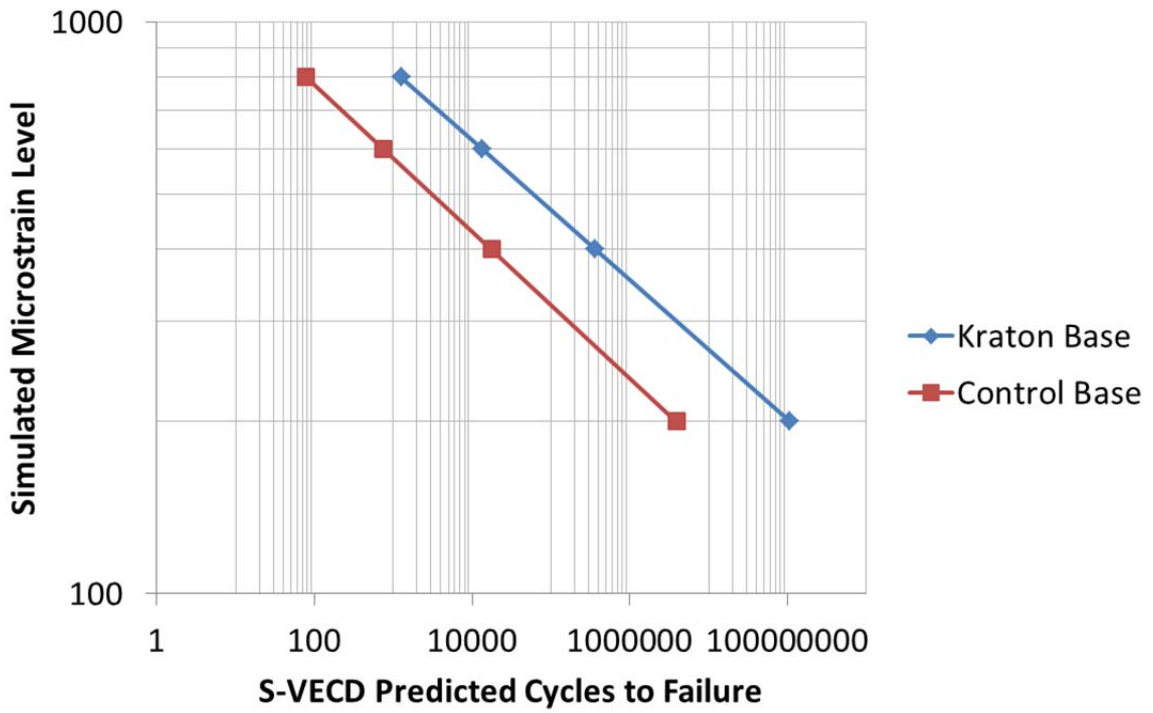
Figure 2.2 Predicted Cycles to Failure

2.2 HWTT Results

Hamburg wheel-track testing (HWTT), shown in Figure 2.3, was performed to determine the rutting and stripping susceptibility of the surface and base mixtures of the Kraton and control test sections. Specimens were prepared, and testing was performed in accordance with AASHTO T 324-04. For each mix, three replicates were tested. Each HWTT replicate consisted of two specimens, with a height between 38 mm and 50 mm, that were cut from a gyratory compacted specimen with a diameter of 150 mm and a height of 95 mm. The air voids of the HWTT specimens were within $7 \pm 1\%$.

The samples were tested under a 158 ± 1 lbs wheel load for 10,000 cycles (20,000 passes) while submerged in a water bath which was maintained at a temperature of 50°C. An LVDT was used to record the relative vertical position of the load wheel after each load cycle. The data were analyzed to determine the point at which stripping occurred in the mixture and the rutting susceptibility of the mixture under loading. Figure 2.4 illustrates typical data output from HWTT. The data show the progression of rut depth with number of cycles. From this curve, two tangents are evident, the steady-state rutting portion of the curve and the portion of the curve after stripping. The intersection of these two curve tangents defines the stripping inflection point (SIP) of the mixture. The slope of the steady-state portion of the curve is multiplied by the number of cycles per hour to determine the rutting rate per hour. Comparing the stripping inflection points and rutting rates of the five different mixtures gives a measure of the relative moisture and permanent deformation susceptibility of the mixture.

Figure 2.3 Hamburg Wheel-Tracking Device

Rut Depth (mm)
30% Rich HB 13A and 13B
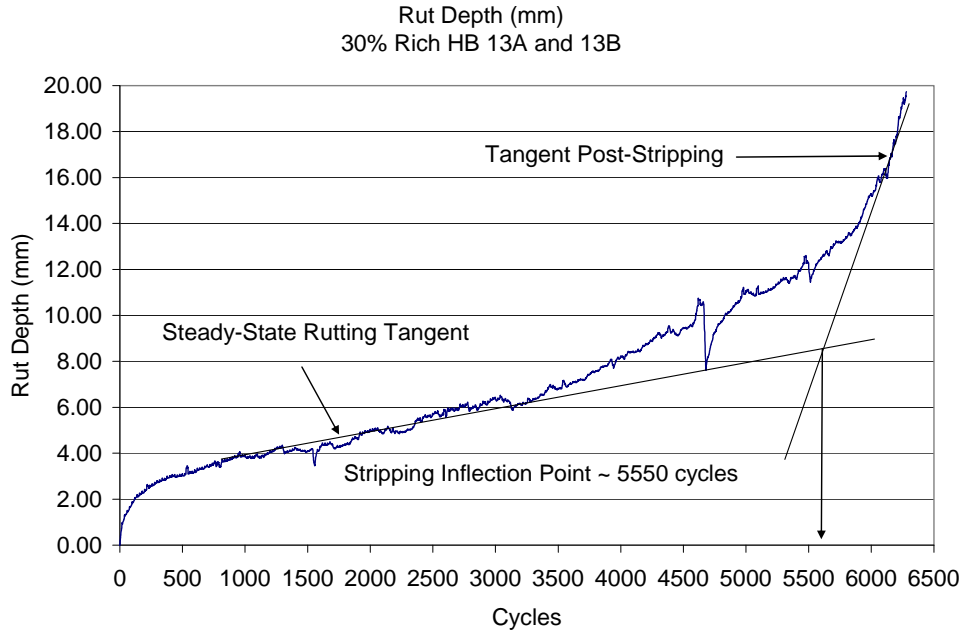
Figure 2.4 Example of Hamburg Raw Data Output

The average SIP's for the four mixtures are shown in Figure 2.5. The error bars represent ± one standard deviation of the test results of three replicates. Numerically, both Kraton mixtures had larger SIP's than either of the control mixtures, with the base mixture not having a measured inflection point during the 10,000 cycle test. However, an ANOVA ($\alpha = 0.05$) showed that only the Kraton base mixture was statistically different from the control mixtures ($p = 0.000$). While there is not a nationally recognized minimum SIP threshold, 5,000 cycles is commonly used as a criterion (Brown et al., 2001). All four mixtures have average SIP values larger than this criterion; therefore, it is expected that none of the mixtures will be prone to moisture damage.
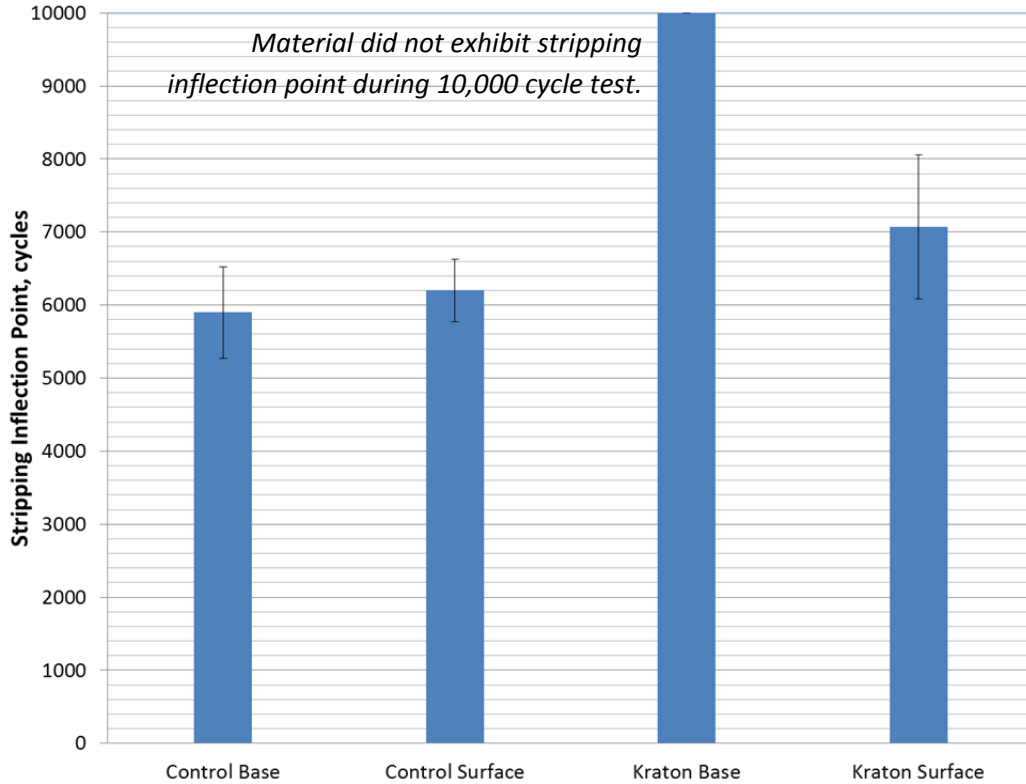
Figure 2.5 SIP from HWTT

The HWTT is also used to characterize an asphalt mixture's ability to resist permanent deformation through measured rut depths and rutting rates. The average rutting rates and rut depths for all four mixtures are shown in Figure 2.6. Smaller rut depths and rates are commonly associated with better resistance to rutting in the field.

While state specific criteria exist, there is no national consensus in terms of maximum allowable rut depths or rutting rate for this testing methodology. As an example of state specific criteria, the State of Texas requires mixtures with a PG 76-XX base binder or higher have less than a 12.5 mm rut depth after 10,000 cycles in HWTT. All the mixtures exhibited the rut depths less than 12.5 mm after 10,000 cycles; hence, none of these mixtures are expected to have a rutting problem in the field.
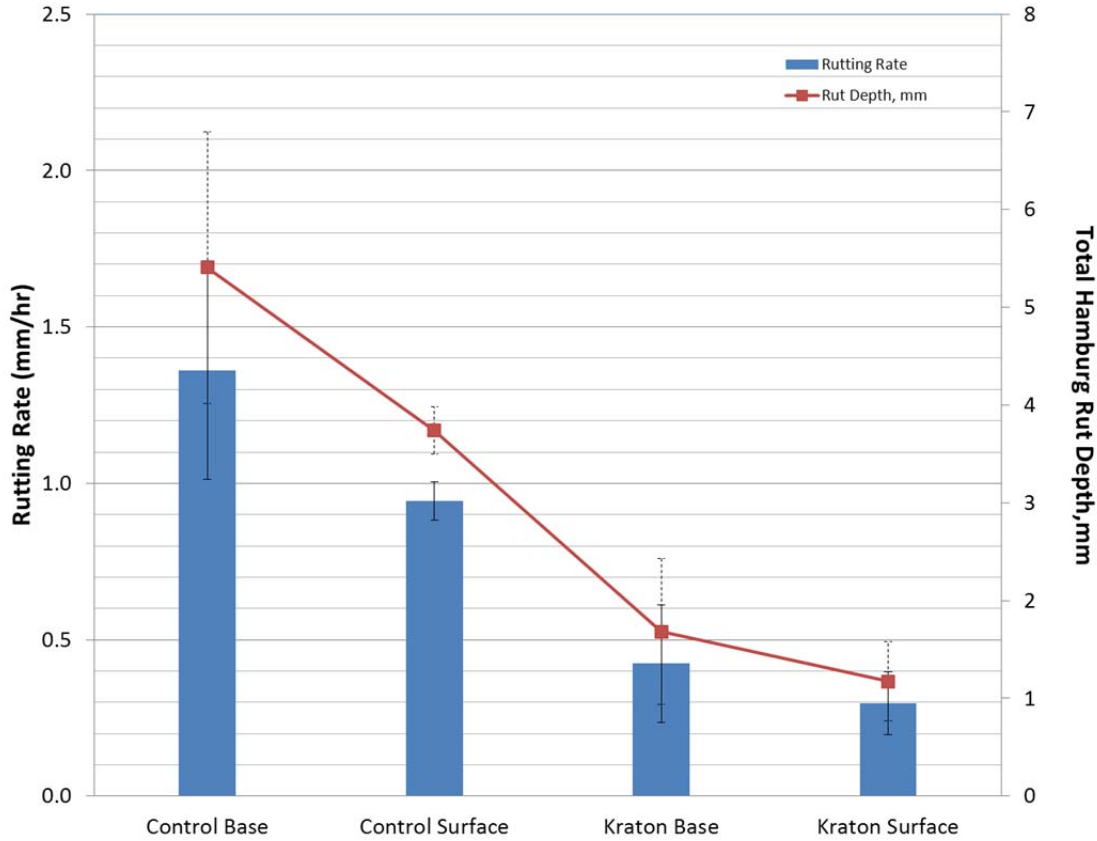
Figure 2.6 Rutting Results from HWTT

An ANOVA ($\alpha = 0.05$) showed no statistical differences between the four mixtures in terms of rut depth ($p = 0.151$); however, there was a statistical difference in the rutting rates of the mixtures ($p = 0.002$). A Tukey-Kramer statistical analysis ($\alpha = 0.05$) was then used to group the mixtures based on the rutting rates. The groupings of the four mixtures are given in Table 2.1. The control surface mixture belonged to both groups, while the Kraton mixtures and the control base were statistically different from each other.

Table 2.1 Tukey-Kramer Results – Rutting Rates

Mixture	Group A	Group B
Control Base	X	
Control Surface	X	X
Kraton Base		X
Kraton Surface		X

3. FALLING WEIGHT DEFLECTOMETER TESTING AND BACKCALCULATION
The 2009 Test Track was opened to traffic on August 28, 2009. Beginning at that time, each section was subjected to falling weight deflectometer (FWD) testing three to four Mondays per month. One Monday per month was reserved for calibration of the FWD equipment. This schedule was necessary because of time constraints and the need to test a total of sixteen sections within the structural experiment. The previous report (Timm et al., 2012) included data through

June 13, 2011. The data presented below include all FWD testing as part of the 2009 experiment.

The FWD was a Dynatest Model 8000 FWD (Figure 3.1). Nine sensors, as listed in Table 3.1, were used with a 5.91 in. radius split plate. Three replicates at four drop heights, listed in Table 3.2, were applied in each FWD test sequence.

Figure 3.1 Dynatest Model 8000 FWD

Table 3.1 FWD Sensor Spacing

Sensor	Offset, in.
1	0
2	8
3	12
4	18
5	24
6	36
7	48
8	60
9	72

Table 3.2 FWD Drop Heights and Approximate Weights

Drop Height	Approximate Weight, lb	Replicates
1	6,000	3
2	9,000	3
3	12,000	3
4	16,000	3

Testing on a particular date consisted of proceeding around the Test Track at a particular offset (inside wheelpath, between wheelpath or outside wheelpath) and stopping at each random location within a section to apply three replicate drops at each of the four drop heights. An entire

offset was tested around the track before progressing to the next offset. This process typically consumed six to eight hours on any given test date. The starting offset was randomized week-to-week to be sure that each offset was tested during different times of the day (morning, mid-day, or afternoon) over the course of all the test dates. In-situ pavement temperatures were recorded for each section at each offset during testing.

Backcalculation of the deflection basins was conducted using EVERCALC 5.0. For both the Kraton and control sections, a three-layer pavement section (AC over aggregate base over subgrade) was simulated. Surveyed layer thicknesses at each offset and random location were used in the backcalculation process. The data presented below represent those deflection basins for which the root mean square error (RMSE) was below 3%.

Figures 3.2, 3.3 and 3.4 summarize the backcalculated results for the AC, granular base and subgrade, respectively. Data points within each plot represent the average backcalculated modulus across the entire test section at the 9,000-lb load level. The seasonal effects of temperature on AC modulus are clearly evident in Figure 3.2 while the unbound materials were largely unaffected by seasonal temperature changes (Figures 3.3 and 3.4). These results are consistent with previous findings at the Test Track (Timm and Priest, 2006; Taylor and Timm, 2009).
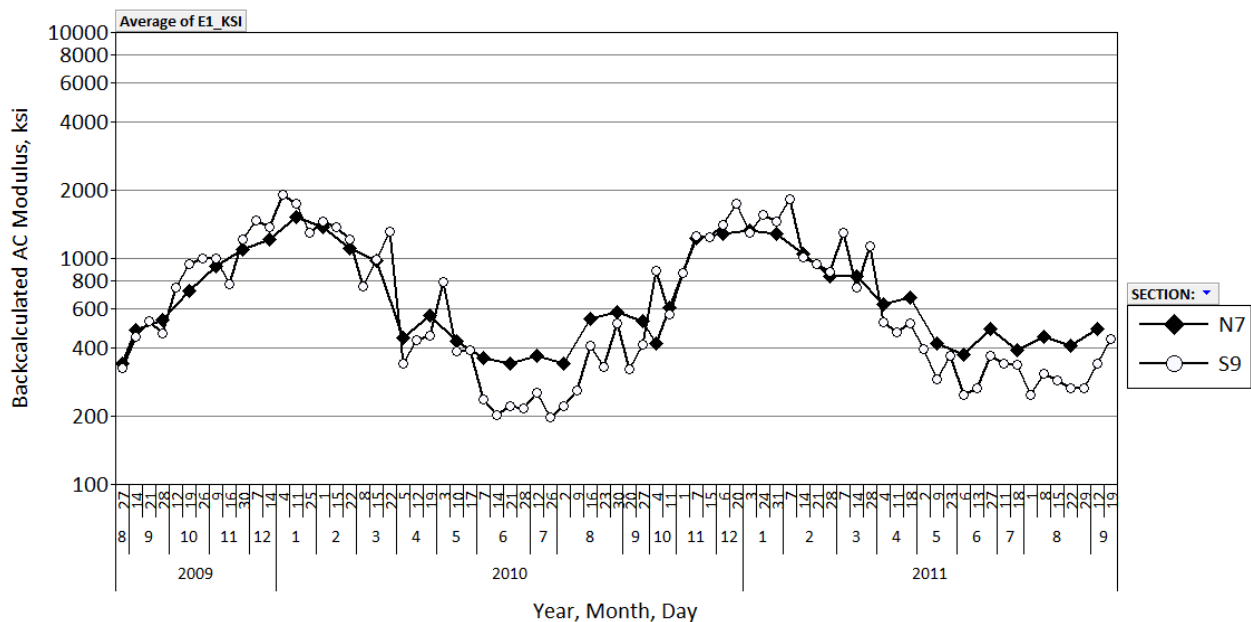
Figure 3.2 Backcalculated AC Modulus vs. Date (Section-Wide Average)
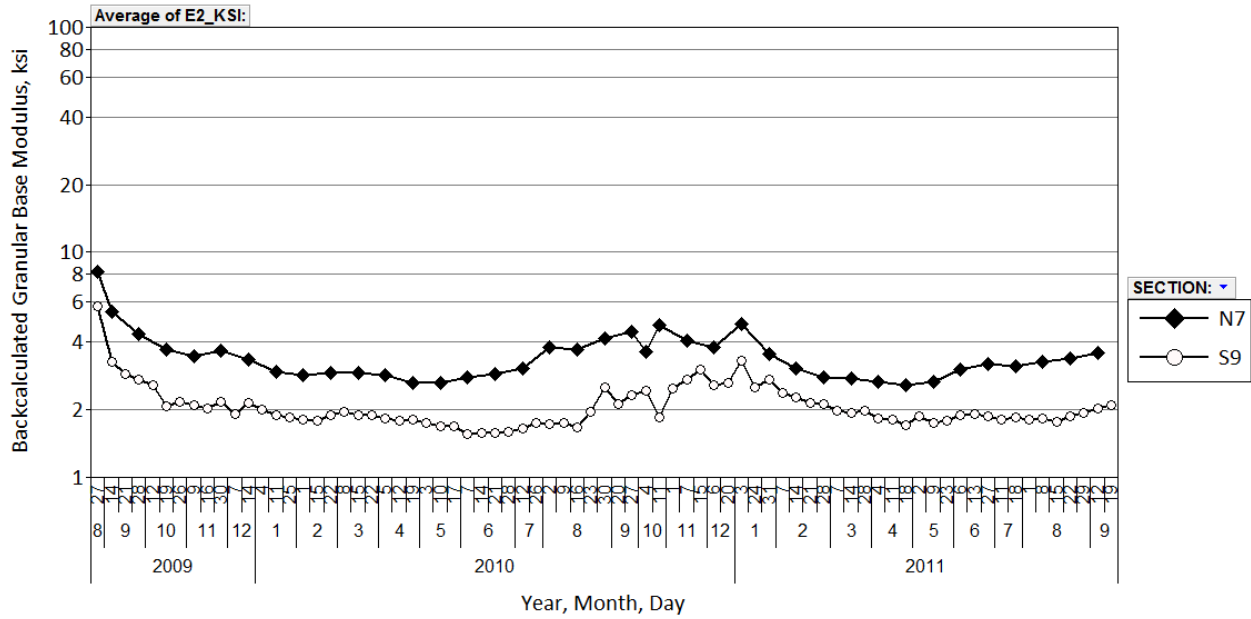
Figure 3.3 Backcalculated Granular Base Modulus vs. Date (Section-Wide Average)
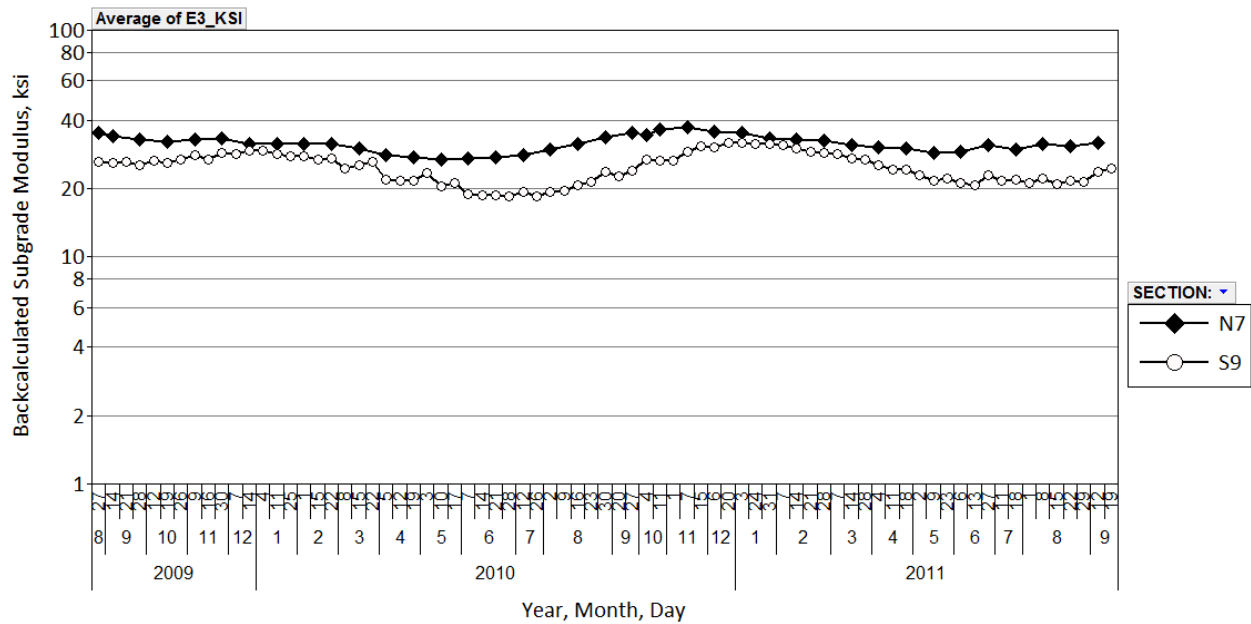
Figure 3.4 Backcalculated Subgrade Soil Modulus vs. Date (Section-Wide Average)

Figure 3.3 shows relatively low granular base moduli in each of the test sections. Though these values may seem artificially low, these are consistent with findings from previous laboratory triaxial resilient modulus testing and values obtained from FWD evaluation at the Test Track on this crushed granite material (Timm and Priest, 2006; Taylor and Timm, 2009). It is also important to note the general decline in granular base modulus during the first few months that occurred in both sections. The reason for this is not immediately clear and will be further investigated upon forensic evaluation in the future.

Figure 3.4 indicates the soil modulus under the Kraton section (N7) was somewhat greater than the soil under the control section (S9). This difference likely resulted from the construction history of the respective sections. Section N7 was placed in a test cell used previously for structural evaluations with relatively thin cross-sections. Therefore, in preparation for paving, N7 only required milling through the previous AC and granular base leaving the subgrade largely intact. This subgrade had been quarried and placed in 2003 from the lower cut of the West curve at the Test Track. Section S9 was placed in a cell that required deep milling (26 inches) of the AC followed by placement and compaction of newly quarried material from the upper hill area of the West curve at the Test Track. Slight differences in materials and duration of consolidation could be responsible for the differences in the subgrade moduli. With respect to structural modeling, the fact that they are different is not as critical as accurately quantifying the difference.

At the time of each FWD test, the mid-depth temperatures were recorded by embedded temperature probes in each section. Figure 3.5 plots the backcalculated AC modulus versus mid-depth temperature for each section in addition to best-fit exponential functions. Figure 3.5 includes the backcalculated AC modulus for each of the three replicates at the 9,000 lb load level, rather than the average AC modulus for a given date, as shown in Figure 3.2. Therefore, there is more scatter in the data than that shown previously in Figure 3.2. Despite the increased scatter, the change in AC modulus was well explained by change in mid-depth temperature ($R^2 \geq$ 0.88). It is interesting to note that the two regression lines cross at approximately 77°F. At cooler temperatures, the control section has higher modulus. At warmer temperatures, the Kraton section had higher modulus. The effect of temperature on modulus was also less on the Kraton material compared to the control section. Despite these differences, the fact that the materials could be modeled in a very similar fashion leads to the conclusion that the Kraton material can be modeled using conventional approaches.
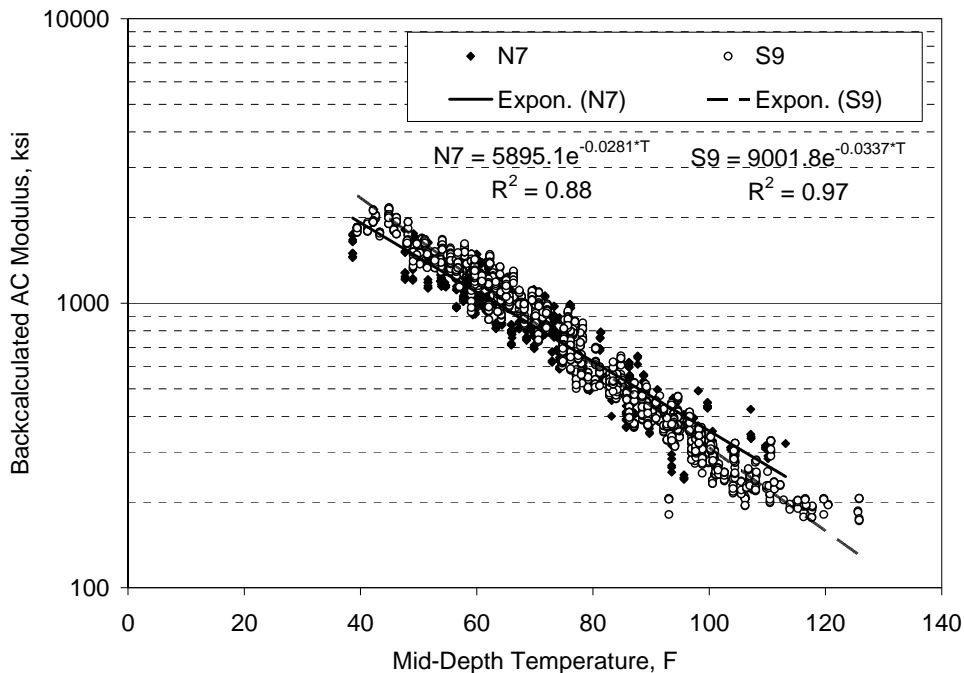
Figure 3.5 Backcalculated AC Modulus vs. Mid-Depth Temperature

To examine the differences between sections in backcalculated AC moduli over a range of temperatures, the moduli were temperature-corrected using the coefficients from Figure 3.5. Three reference temperatures were selected (50, 68 and 110°F) that represented the range of FWD test temperatures. As noted in Figure 3.5, each data set was fitted by an exponential function:

$$E = \alpha_1 e^{\alpha_2 T}$$ (3.1)

where:
E = backcalculated AC modulus, ksi
T = mid-depth pavement temperature, °F
α_1, α_2 = best-fit regression constants

Equation 3.1 has been used in previous Test Track research cycles to characterize the modulus-temperature relationship for both laboratory and field-determined moduli (Timm and Priest, 2006; Taylor and Timm, 2009). A temperature-corrected AC modulus (E_{Tref}) was determined from Equation 3.1 at a given reference temperature (T_{ref}) by dividing Equation 3.1 at T_{ref} by the same equation at the measured temperature (T_{meas}). After canceling terms and solving for E_{Tref}, the following equation was determined:

$$E_{T_{ref}} = E_{T_{meas}} e^{\alpha_2 \left(T_{ref} - T_{meas}\right)}$$ (3.2)

Equation 3.2 illustrates that the key variable in performing the temperature correction is the exponential regression coefficient, α_2. The results of temperature-correction are summarized in Figure 3.6.

Figure 3.6 shows the average, standard deviation and coefficient of variation (COV) of each section's AC modulus at each reference temperature. In each case, the COV was less than 30%, which is a common benchmark for backcalculated AC modulus variability (Allen and Graves, 1994; Noureldin, 1994; Timm et al., 1999). Therefore, the AC moduli appear remarkably consistent within each section.
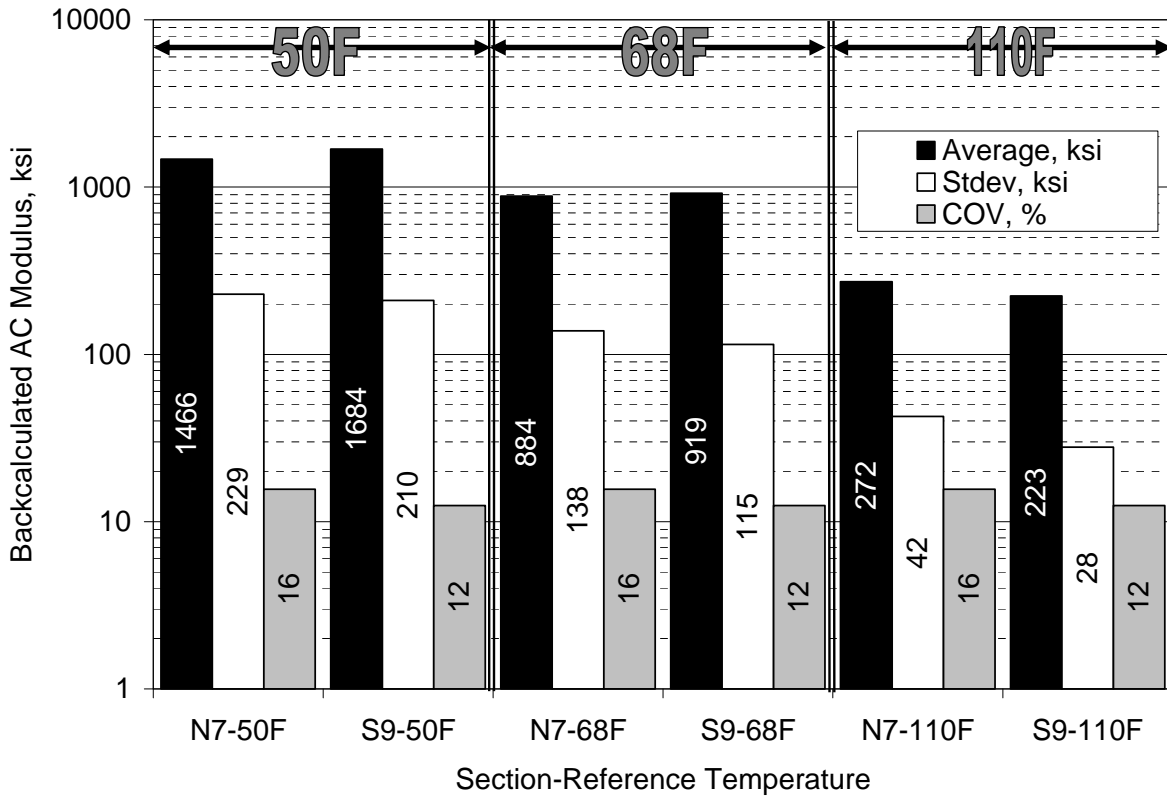
Figure 3.6 Backcalculated AC Modulus Corrected to Reference Temperatures

Statistical testing was conducted using a two-tailed Students' t-test ($\alpha = 0.05$) assuming unequal variance with the null-hypothesis that the mean values were equivalent between sections at each reference temperature. The mean backcalculated moduli, at each reference temperature in Figure 3.6, were found to be statistically different. At 50 and 68°F, the control section had statistically higher modulus. At 110°F, the reverse was true.

A final step in this analysis was to plot, in Figure 3.7, backcalculated AC modulus at 68°F versus date to look for changes in AC modulus that would indicate possible pavement distress or short term aging. Trendlines were fit to both sections' data resulting in positive slopes with very low corresponding R^2. This result indicates that neither section seems to be experiencing structural distress and only very minor aging over time. Further monitoring is recommended to track longer-term aging.
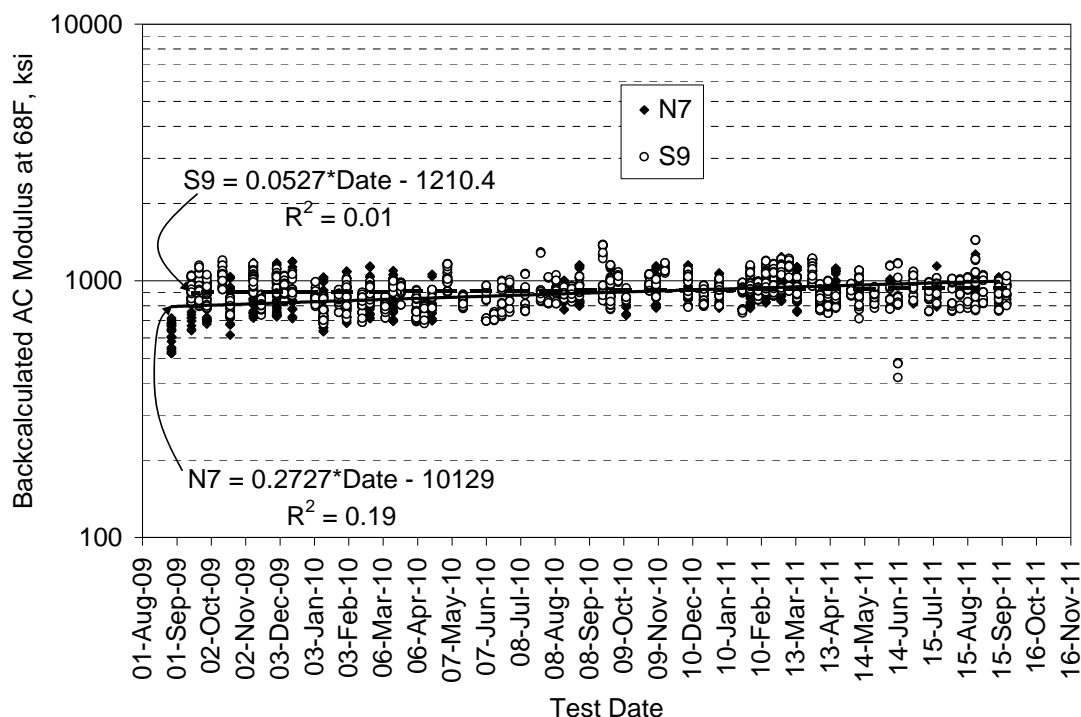
Figure 3.7 Backcalculated AC Modulus vs. Date at 68°F

4. PAVEMENT RESPONSE MEASUREMENTS

As noted previously, traffic began on August 28, 2009. At that time, weekly pavement response measurements using the embedded asphalt strain gauges and earth pressure cells in the granular base and subgrade soil commenced. Weekly data collection consisted of collecting approximately fifteen truck passes (three passes of five trucks) in each section. The frequency of testing and number of trucks collected were consistent with previous data collection efforts at the Test Track which were shown to be sufficient to capture daily variability, seasonal variability and wheel wander effects (Timm and Priest, 2005; Priest and Timm, 2006). The response data in the previous report (Timm et al., 2012) were gathered between August 28, 2009 and June 9, 2011. The data presented below represent all data gathered as part of the 2009 experiment.

Strain and pressure readings were acquired using a DATAQ DI-785 data acquisition system at a frequency of 1,000 samples/second/gauge. Raw signals were recorded in voltage versus time, and customized processing templates developed in DaDISP were developed to clean the signals using a frequency filter, determine the peak responses for a given truck pass, and convert the voltage output into engineering units of stress or strain, as appropriate. Figure 4.1 shows a sample truck pass over the aggregate base and subgrade soil earth pressure cells. The signals are in voltage versus time with peaks noted for each axle in the tractor-trailer combination. The processing scheme tabulates the peak responses, relative to the baseline, for each axle pass.
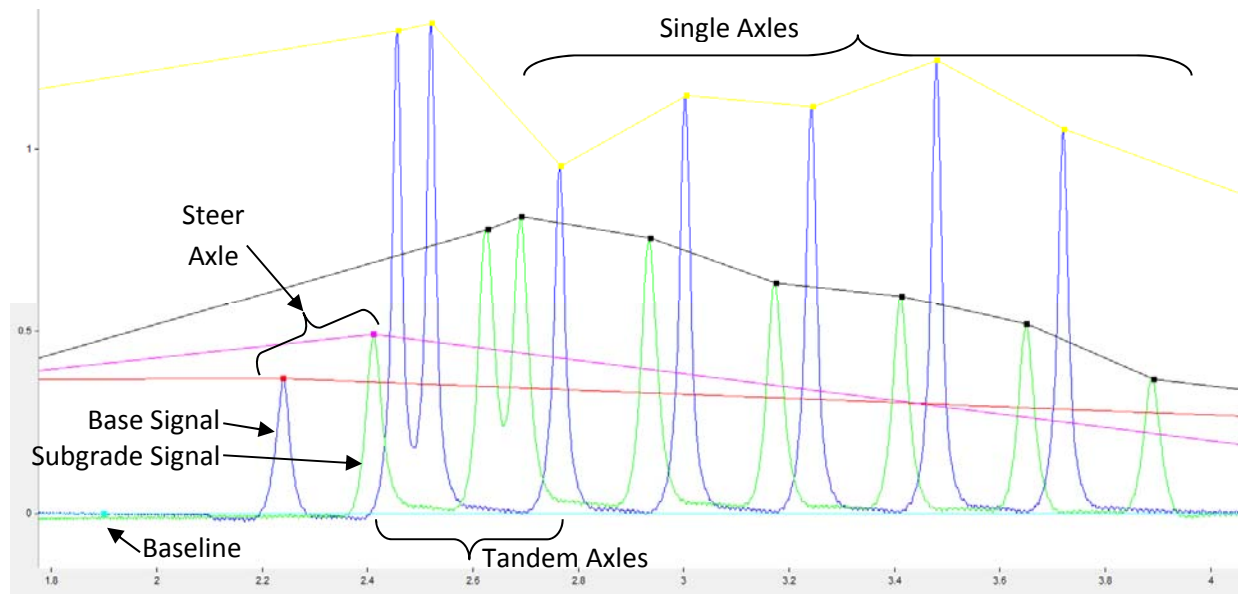
Figure 4.1 DaDISP Screen Capture of Pressure Measurements for Truck Pass

Figures 4.2 and 4.3 show typical strain response measurements in the longitudinal and transverse directions, respectively. The longitudinal measurements (Figure 4.2) usually have compressive strain as the axle approaches the gauge followed by peak tensile response when the axle is directly over the gauge. Finally, the pavement again goes into compression as the axle departs. This cyclic effect is seen throughout each of the axle passes in Figure 4.2.

Transverse strain responses (Figure 4.3) were distinctly different than the longitudinal strain measurements. The processing scheme was the same as that described above, but the signals typically were unilaterally compressive or tensile without the strain reversal seen in the longitudinal measurements. Full explanation of this behavior has been documented previously (Timm and Priest, 2008).

For each truck pass on each gauge, maximum (tensile) and minimum (compressive) responses, in addition to the amplitude (maximum-minimum) for each axle were recorded relative to the baseline. An Access database system was used to archive the data from which the "best-hit" response on a given day was determined on an axle-type basis. The "best-hit" represents the 95th percentile reading on a particular test day from all the readings made under a particular axle type. For example, on a typical day there could be 450 longitudinal strain readings made under single axles in a particular section (6 longitudinal gauges∗5 trucks∗3 passes/truck∗5 single axles/truck = 450 strain readings). The 95th percentile of these 450 readings represented the "best-hit" response for longitudinal strain.   The 95th percentile was used in previous research cycles at the Test Track (Willis and Timm, 2009) and was found to reasonably represent the true best-hit but guard against erroneously-high readings. This same approach was used for all axle types and the other measurements (base pressure, subgrade pressure and transverse strain).
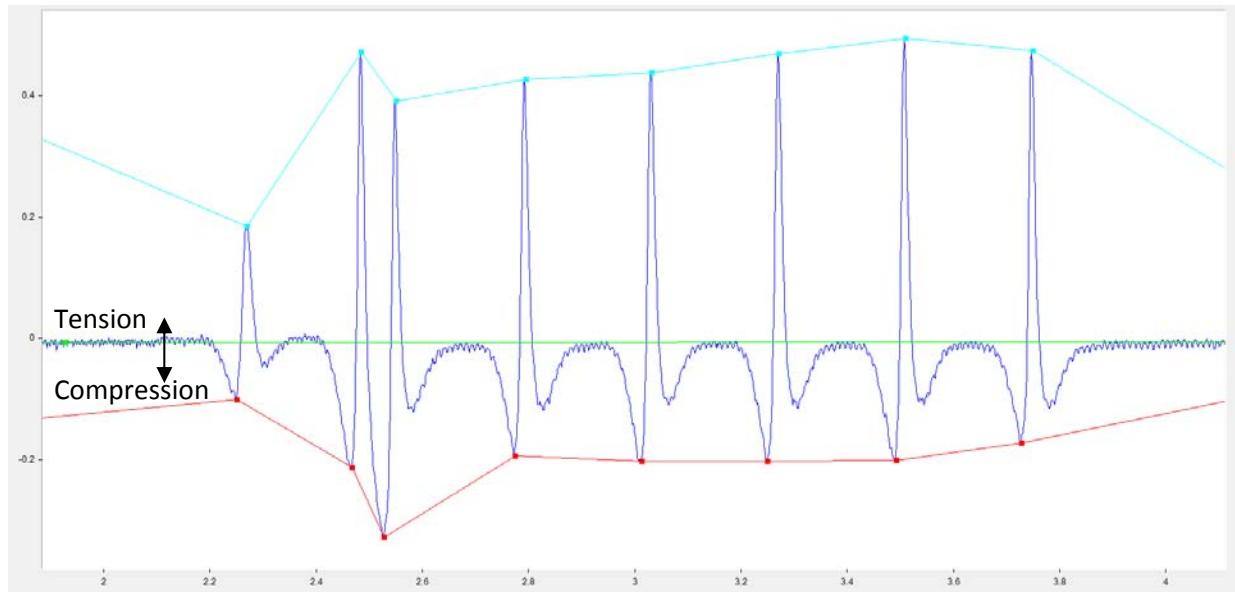
Figure 4.2 DaDISP Screen Capture of Longitudinal Strain Measurements
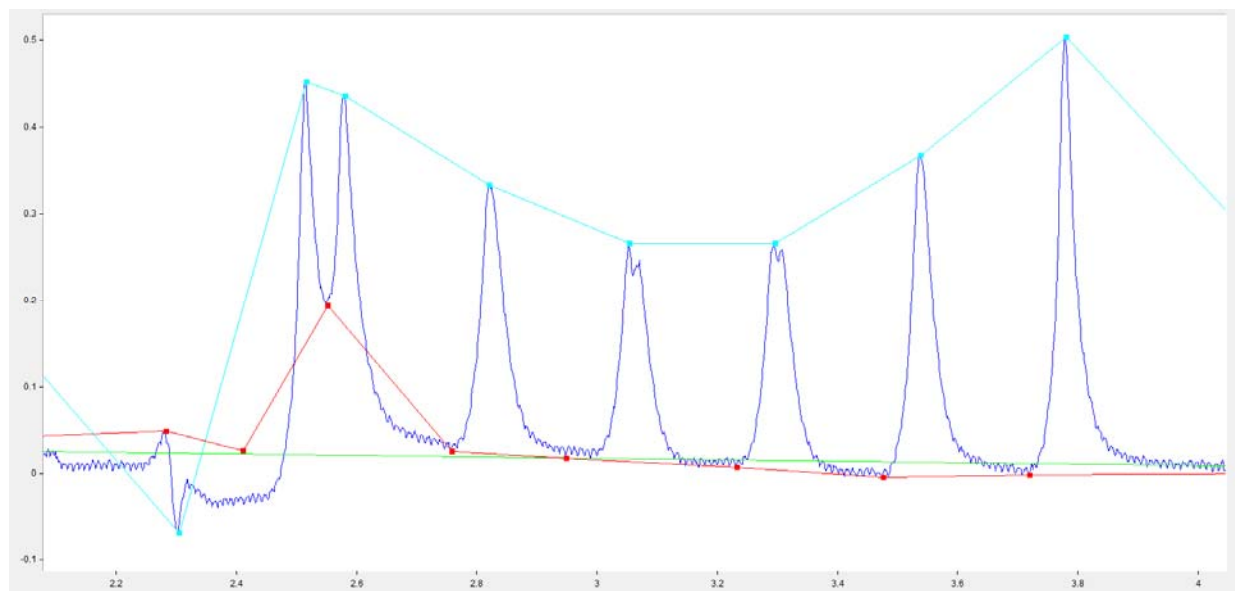
Figure 4.3 DaDISP Screen Capture of Transverse Strain Measurements

After collecting, processing, and archiving the data, there were a number of analyses conducted. The following subsections examine seasonal trends in pavement response, temperature effects on pavement response, responses normalized to particular reference temperatures, responses over time at a normalized temperature and distributions of pavement response.

4.1 Seasonal Trends in Pavement Response

As discussed above, there are four primary measured pavement responses: longitudinal strain in the AC, transverse strain in the AC, vertical pressure in the aggregate base, and vertical pressure in the subgrade soil. Figures 4.4 through 4.7 plot these responses versus test date for the single axle loadings only, although similar trends were observed with the other axle types. Each data point in each plot represents the "best-hit" on that particular test date. The seemingly large

fluctuation in strain between consecutive test dates is a product of alternating collection times between morning and afternoon on a week-to-week basis. This ensures that a fuller range of temperatures are sampled during a particular season.

In each plot, the seasonal trends are clearly evident with lower responses during the cooler months and increased responses during warmer months. It was noted in the previous report (Timm et al., 2012) that the longitudinal and transverse strain measurements became more erratic over time while this wasn't necessarily true for the pressure measurements. It should be further noted that very few strain readings were obtained toward the end of the experiment in the Kraton section due to gauges going offline or becoming excessively erratic. This appears to be related strictly to the gauges themselves and not reflective of pavement performance.
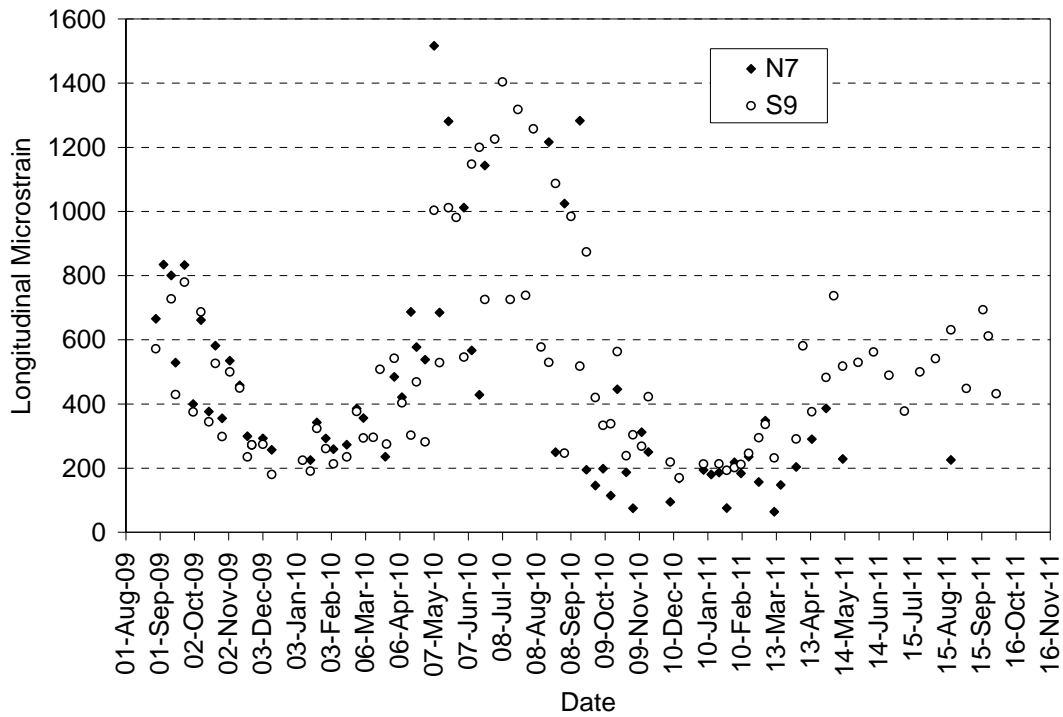
Figure 4.4 Longitudinal Microstrain Under Single Axles
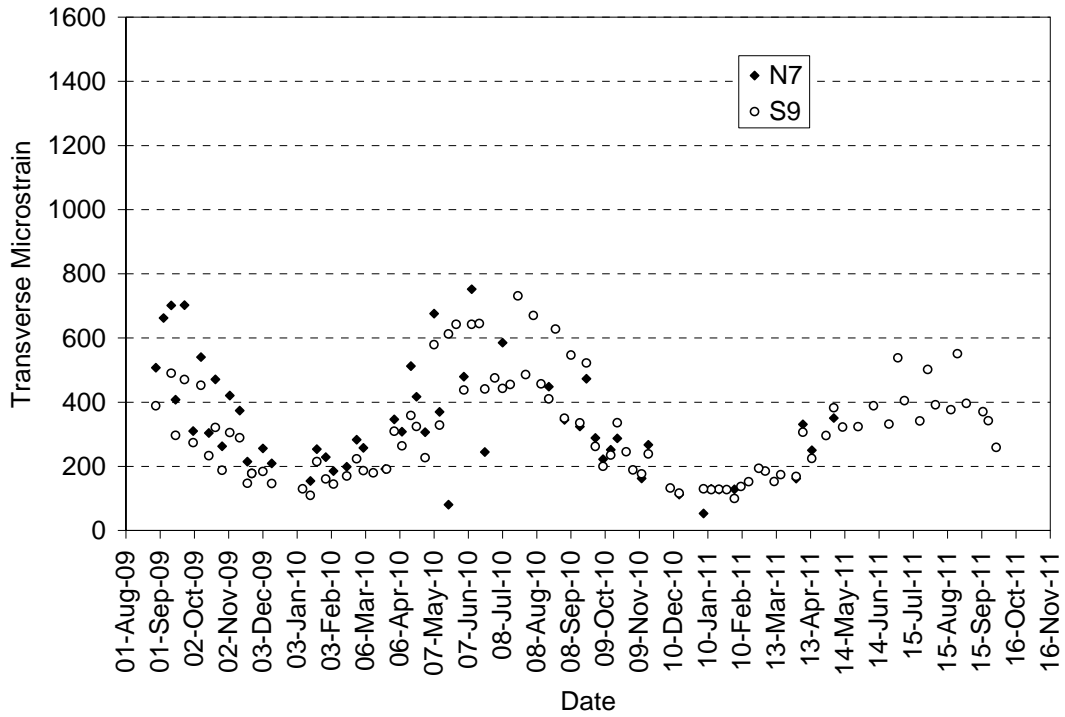
Figure 4.5 Transverse Microstrain Under Single Axles
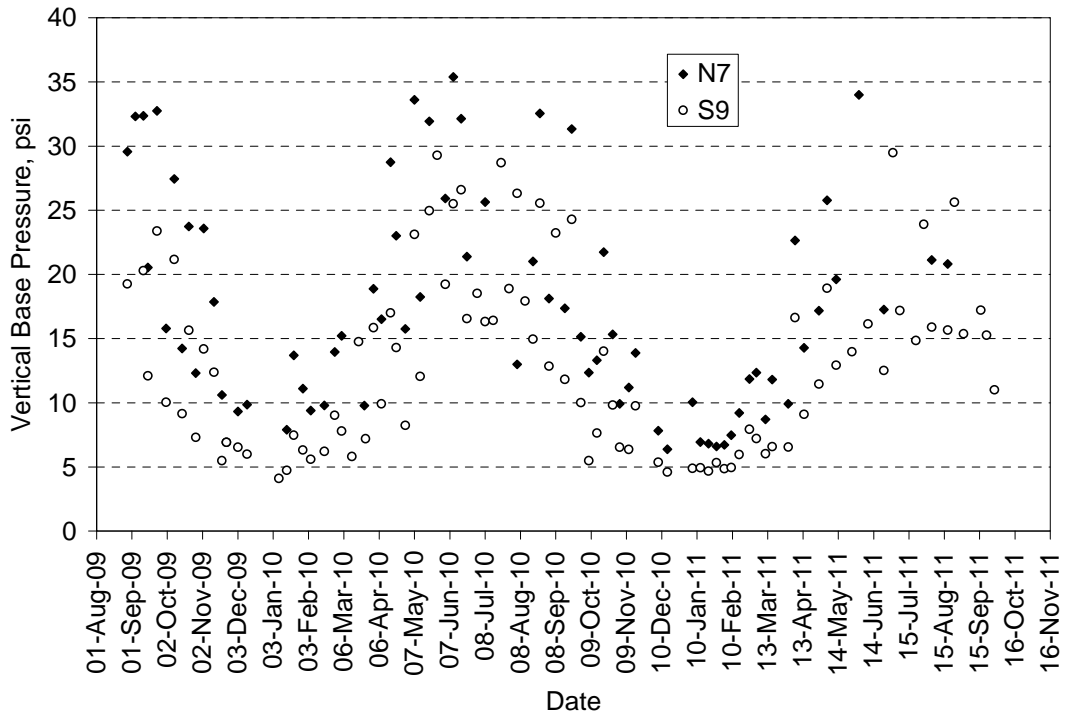
Figure 4.6 Aggregate Base Pressure Under Single Axles
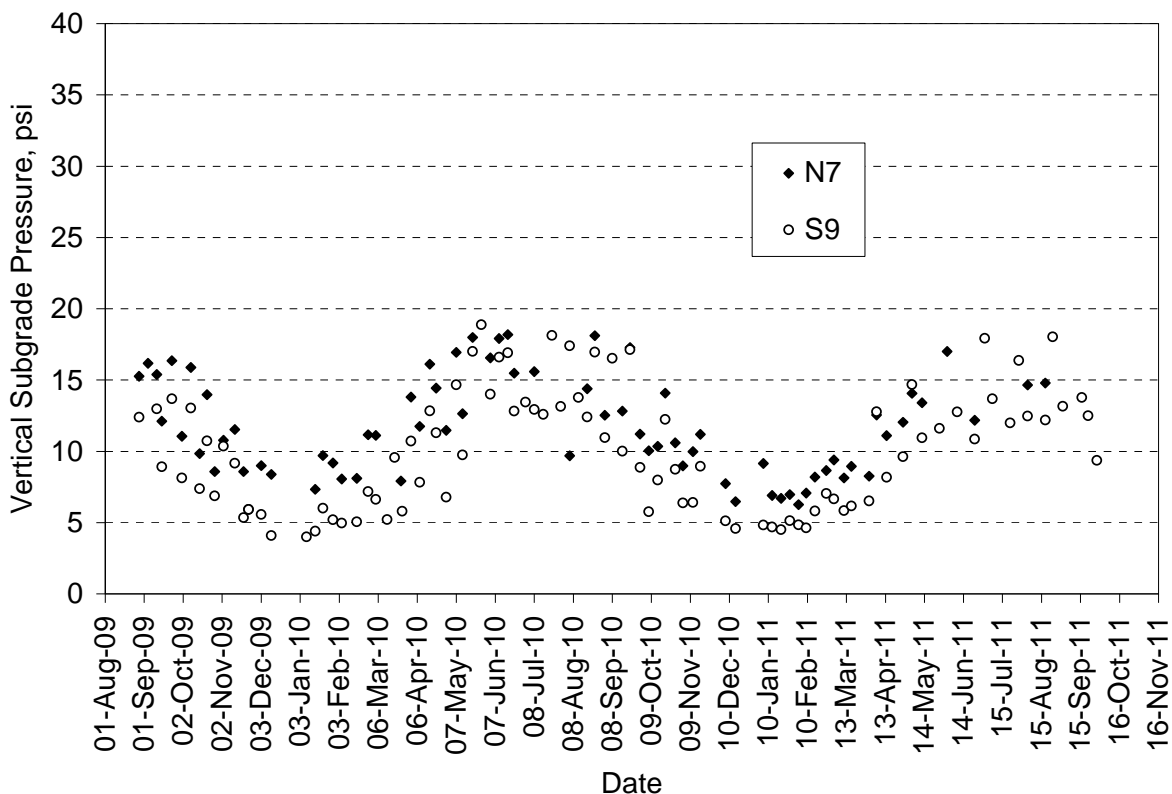
Figure 4.7 Subgrade Pressure Under Single Axles

4.2 Pavement Response vs. Temperature

The data presented in Figures 4.4 through 4.7 were the best-hit pavement responses on a particular test date. These data were re-plotted in Figures 4.8 through 4.11 against their corresponding mid-depth pavement temperature. Exponential regression equations, much like those determined for the backcalculated AC moduli, were best-fit to each data set in Figures 4.8 through 4.11, representing single axles. Furthermore, a cutoff date of April 21, 2010 (21-APR-10) was used to separate "clean" from "erratic" strain data. In the previous report (Timm et al., 2012), a cutoff date in mid-February was used. However, after reviewing the entire data set, it appeared that mid-April was more appropriate and would include more data in the analysis.

Figures 4.8 and 4.9 include regression equations for the entire N7 data sets through April 21, 2010 for longitudinal and transverse strain, respectively. In the case of longitudinal strain (Figure 4.8) the N7 curve from the reduced data set was much higher than its counterpart using all the data and also higher than the control section's curve. This was expected since N7 was purposely built thinner than the control which should result in higher strain levels. The effect of using the cutoff date was similar for transverse strain (Figure 4.9). In both cases, the R^2 also improved dramatically, as expected.

Figures 4.10 and 4.11 show generally strong trends between temperature and vertical pressure for both sections. The increased base pressure (Figure 4.10) in N7 was again expected due to less AC thickness than the control. It is interesting to note that the subgrade pressure (Figure

4.11) in roughly equivalent to the control at high temperatures. This may have resulted from the increased modulus of the Kraton material, relative to the control, at high temperatures.
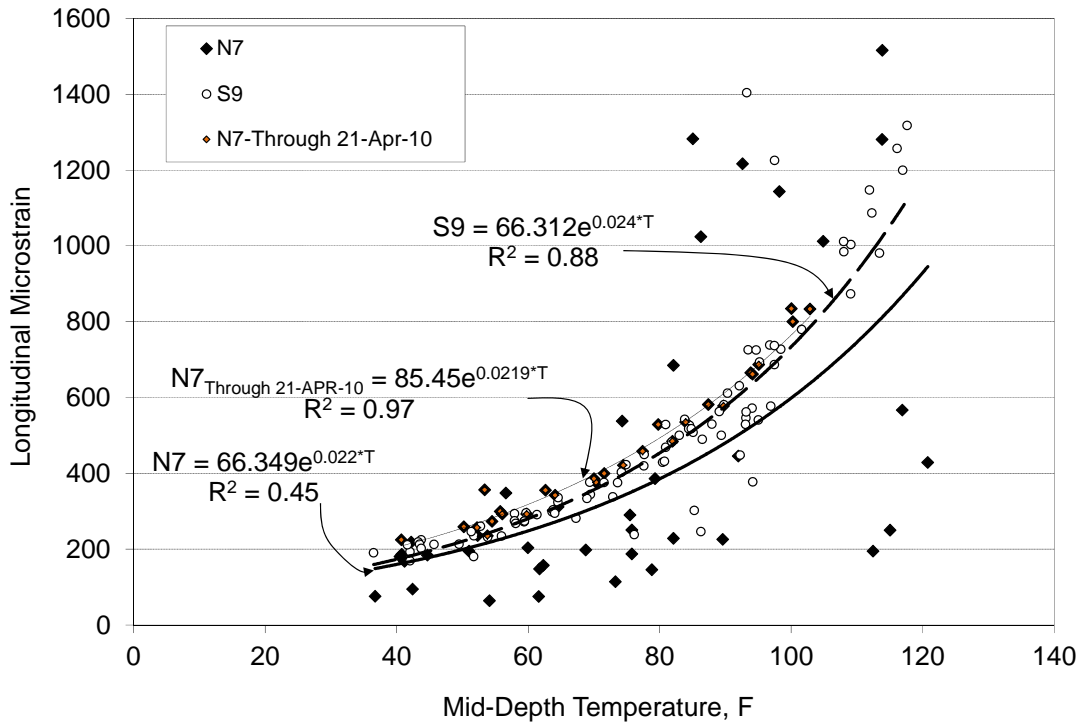
Figure 4.8 Longitudinal Strain vs. Mid-Depth Temperature Under Single Axles
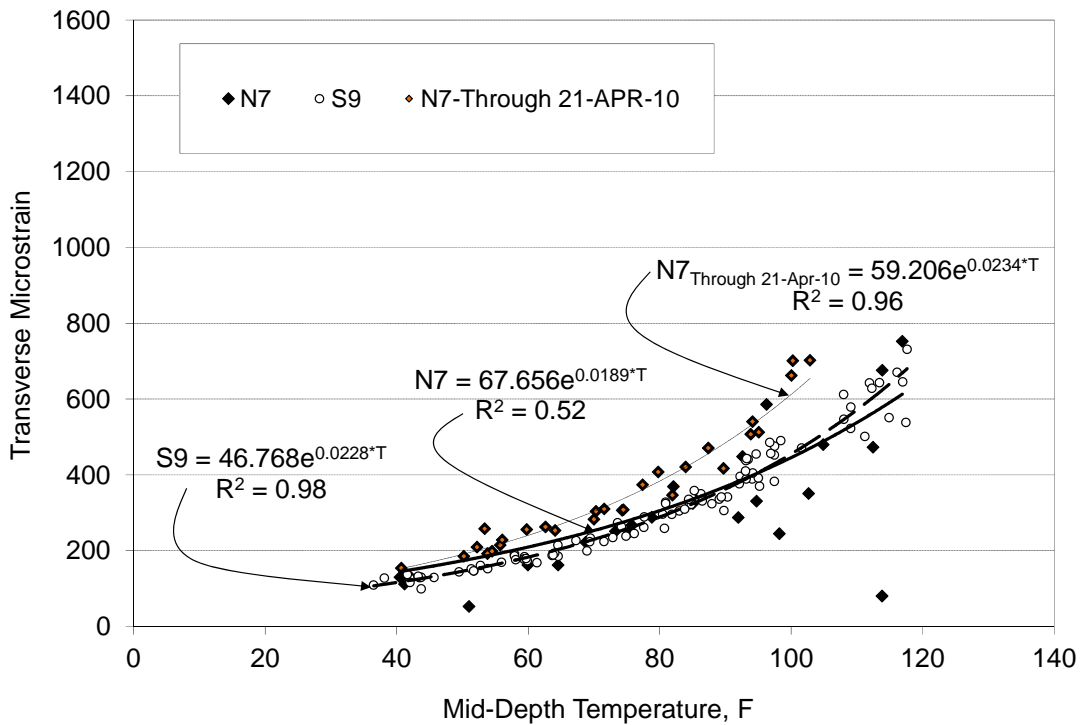
Figure 4.9 Transverse Strain vs. Mid-Depth Temperature Under Single Axles
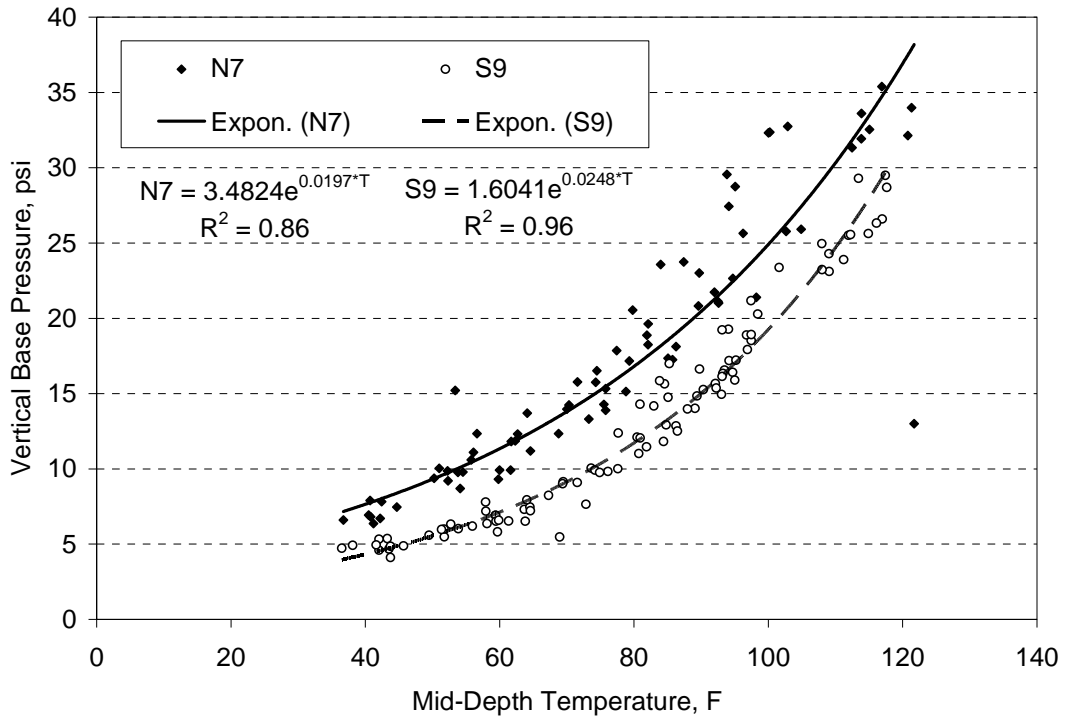
Figure 4.10 Base Pressure vs. Mid-Depth Temperature Under Single Axles

In the plot: legend entries N7 (filled diamond), S9 (open circle), Expon. (N7) solid line, Expon. (S9) dashed line.

$N7 = 3.4824e^{0.0197*T}$ $S9 = 1.6041e^{0.0248*T}$
$R^2 = 0.86$ $R^2 = 0.96$

Axis labels: Vertical Base Pressure, psi (y-axis); Mid-Depth Temperature, F (x-axis).
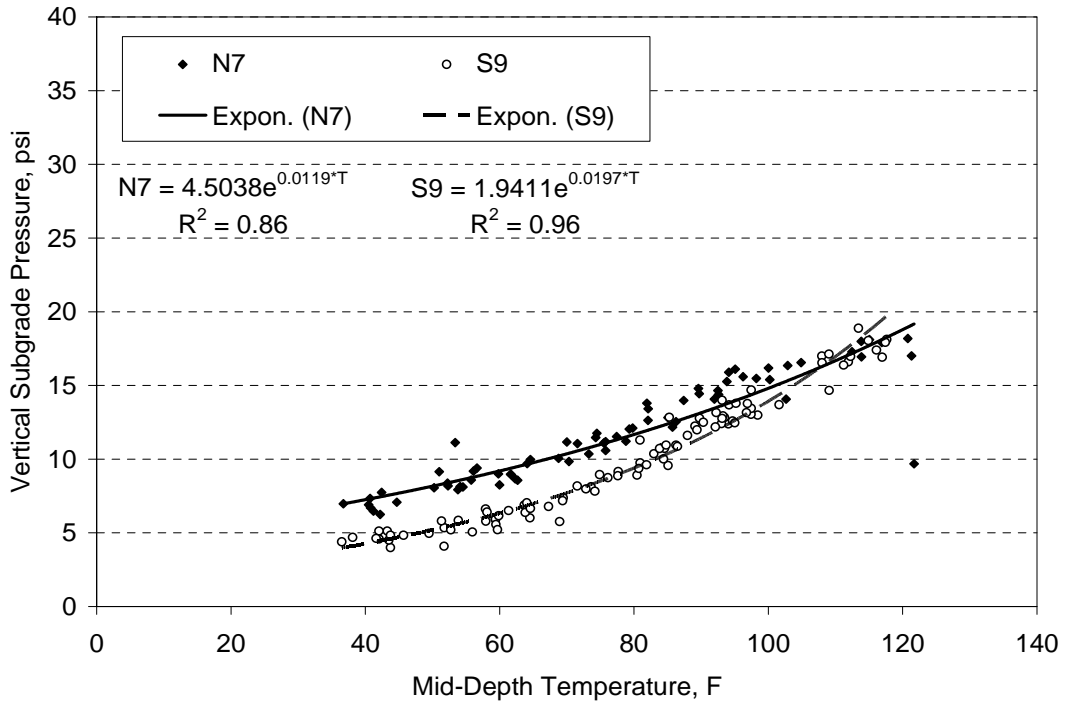
Figure 4.11 Subgrade Pressure vs. Mid-Depth Temperature Under Single Axles

Legend entries N7 (filled diamond), S9 (open circle), Expon. (N7) solid line, Expon. (S9) dashed line.

$N7 = 4.5038e^{0.0119*T}$ $S9 = 1.9411e^{0.0197*T}$
$R^2 = 0.86$ $R^2 = 0.96$

Axis labels: Vertical Subgrade Pressure, psi (y-axis); Mid-Depth Temperature, F (x-axis).

Additional equations were developed for each of the axle types, the results of which are presented in Table 4.1. For the control section, all R^2 values were above 75%. In contrast, within strain measurements for N7, each of the six regression equations had R^2 below 53% indicating a generally poor fit to the exponential equation. Within pressure measurements, only the steer axles R^2 values were below 70%. Clearly, the data were more scattered within the Kraton section, with particularly high scatter seen within the strain measurements. Also included in Table 4.1 are exponentially-fit parameters, using data only through April 21, 2010, for the axle types and responses that had R^2 less than 70%. Subsequent analyses on the single axle responses used the regression equations developed from N7 using the cutoff date.

Table 4.1 Pavement Response vs. Temperature Regression Terms

Section	Axle	Dates	Longitudinal Strain			Transverse Strain			Base Pressure			Subgrade Pressure		
			k_1	k_2	R^2	k_1	k_2	R^2	k_1	k_2	R^2	k_1	k_2	R^2
N7 (Kraton)	Steer	All	22.8912	0.0274	0.43	51.9353	0.0161	0.11	1.8499	0.0200	0.39	2.192	0.013	0.46
		Through 4/21/10	33.2432	0.0284	0.95	39.8294	0.0279	0.88	1.0456	0.0291	0.89	1.8175	0.0151	0.69
	Single	All	66.3493	0.0220	0.45	67.6557	0.0189	0.52	3.4824	0.0197	0.86	4.504	0.012	0.86
		Through 4/21/10	85.4502	0.0219	0.97	59.2056	0.0234	0.96	NA			NA		
	Tandem	All	45.1053	0.0263	0.50	28.1504	0.0260	0.25	4.3109	0.0172	0.71	4.795	0.011	0.75
		Through 4/21/10	68.9054	0.0244	0.98	59.3847	0.0224	0.95	NA			NA		
S9 (Control)	Steer	All	28.3361	0.0276	0.81	26.1178	0.0298	0.94	0.7830	0.0239	0.76	0.867	0.021	0.83
	Single		66.3116	0.0240	0.88	46.7681	0.0228	0.98	1.6041	0.0248	0.96	1.941	0.020	0.96
	Tandem		49.3321	0.0268	0.88	47.2756	0.0221	0.97	1.9967	0.0228	0.95	2.482	0.017	0.95

Gray shading = $R^2 < 0.70$

4.3 Pavement Responses Normalized to Reference Temperatures

To characterize statistical differences in pavement response between sections, temperature corrections were applied to each data set (longitudinal strain, transverse strain, base pressure, subgrade pressure) at 50, 68 and 110°F. The regression terms presented in Table 4.1, using the cutoff date for the strain measurements, were used for this part of the analysis. For both sections, temperature-corrected responses were determined according to:

$$response_{T_{ref}} = response_{T_{meas}} e^{k_2 (T_{ref} - T_{meas})} \tag{4.1}$$

where:
$response_{Tref}$ = response at T_{ref}
$response_{Tmeas}$ = response at T_{meas}
T_{ref} = mid-depth reference temperature (50, 68, 110°F)
T_{meas} = mid-depth measured temperature, F
k_2 = section, axle and response-specific regression constant from Table 4.1

The average, standard deviation, and coefficient of variation were determined at each reference temperature. Two-tailed t-tests (α=0.05) were conducted at each reference temperature to establish statistical significance between average measured responses. Only results for the single axles are presented here, although similar trends were noted amongst the other axles.

4.3.1 Longitudinal Strain Responses

Figure 4.12 summarizes the average, standard deviation, and coefficient of variation (COV) at each reference temperature. The variability, as measured by the COV, was more than double for S9 relative to N7 due to utilizing the cutoff date which eliminated much of the scattered data from N7. At the two lower temperatures, the N7 strain level was statistically higher than the S9 strain level. This was expected since N7 was built thinner and the backcalculated moduli, as presented previously, were lower at these two temperatures. However, at 110°F, N7 and S9 were separated by only 5 με which was not statistically significant. This observation is important since the total N7 AC thickness was approximately 1.25 inches less than S9 which implies that the increase in the N7 AC modulus at the highest temperature was enough to overcome the thickness advantage held by S9.
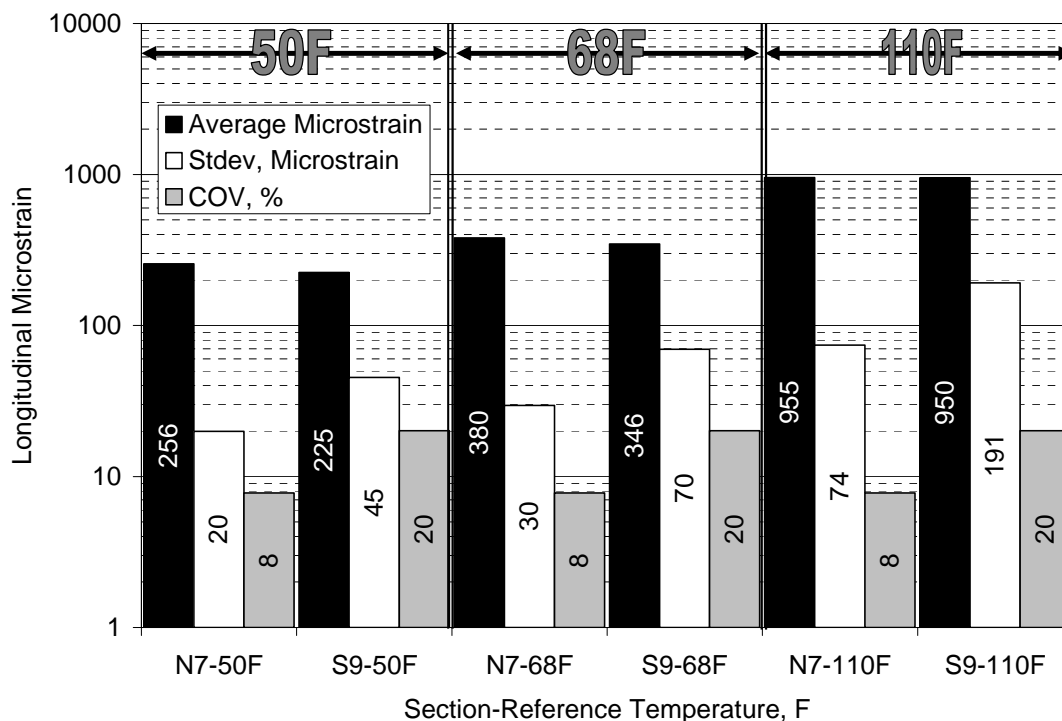
Figure 4.12 Longitudinal Strain Under Single Axles at Three Reference Temperatures

At the conclusion of trafficking no fatigue cracking was evident. However, fatigue estimates can be made for comparison purposes to evaluate relative performance estimates using the strain data in Figure 4.12 with the fatigue transfer functions developed previously in the laboratory. Table 4.2 lists the measured average strain at 68°F and the corresponding predicted fatigue life using the transfer functions presented in the previous report. It is important to note that despite N7 having statistically higher strain levels at 68°F, the improved fatigue characteristics of the Kraton base mixture yields an improvement of approximately 17 times in the predicted fatigue life over the control section.

Table 4.2 Predicted Fatigue Life at 68°F

Section	Average Measured Microstrain at 68F	Predicted Fatigue Life – Cycles to Failure at 68F Using Laboratory-Determined Transfer Function
N7 (Kraton)	380	6,515,371
S9 (Control)	346	367,056

4.3.2 Transverse Strain Responses

Figure 4.13 summarizes the transverse strains under single axle loadings. As found in previous studies (Timm and Priest, 2008), the transverse strains were generally lower than their longitudinal counterparts. Also, the transverse strains in S9 were somewhat more consistent than longitudinal with COV's. Due to this consistency in the transverse strains, differences between sections were more easily detected. At each temperature, differences in average values were statistically different when using a two-sample t-test assuming unequal variance ($\alpha = 0.05$). The fact that the control section was lower than the Kraton section can be attributed primarily to its increased thickness.
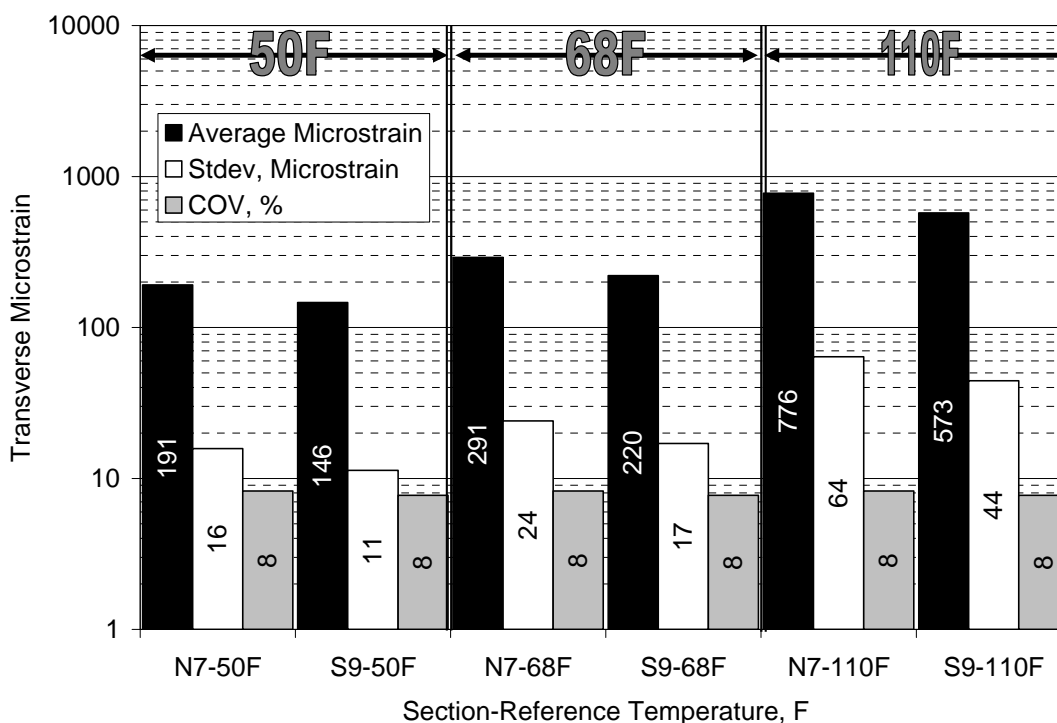
Figure 4.13 Transverse Strain Under Single Axles at Three Reference Temperatures

4.3.3 Aggregate Base Vertical Pressure Responses

Figure 4.14 summarizes the vertical pressures in the aggregate base under single axle loads. The consistency within the data sets certainly contributes to the statistically-significant mean values detected through two-tailed t-tests assuming unequal variance ($\alpha = 0.05$). At each temperature, the control section had lower vertical stress in the base layer than the Kraton section. The primary reason for these differences, as expected, was the increased thickness in the control section. In this case, the increased modulus of the Kraton material at the high temperature was not enough to overcome the thickness disadvantage.
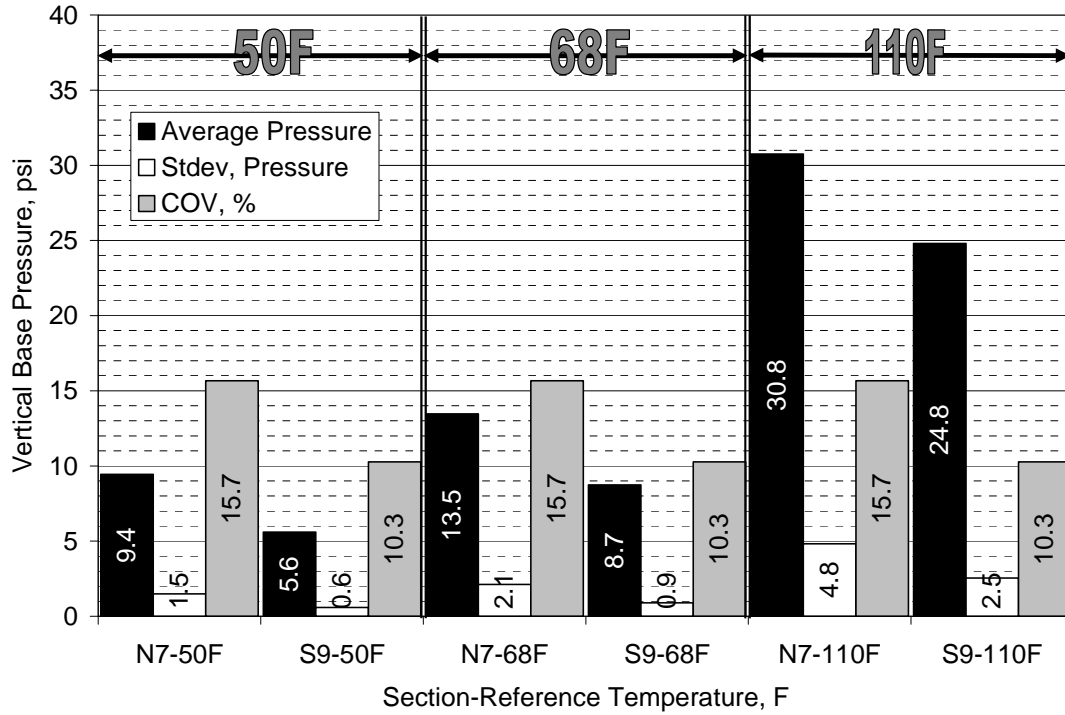
Figure 4.14 Base Pressure Under Single Axles at Three Reference Temperatures

*4.3.4 Subgrade Vertical Pressure Response*s
The temperature-corrected vertical pressures in the subgrade are plotted in Figure 4.15. The mean values at 50 and 68°F in Figure 4.15 are statistically significantly different (two-tailed t-test assuming unequal variance (α = 0.05)). Again, the thickness difference between the two sections, at higher modulus of the control section at the two lower temperatures, explains these results. Interestingly, at 110°F, the mean values are the same. In this case, the increased modulus of the Kraton material at 110°F was sufficient to equalize pressures at this depth despite having a thinner pavement structure.
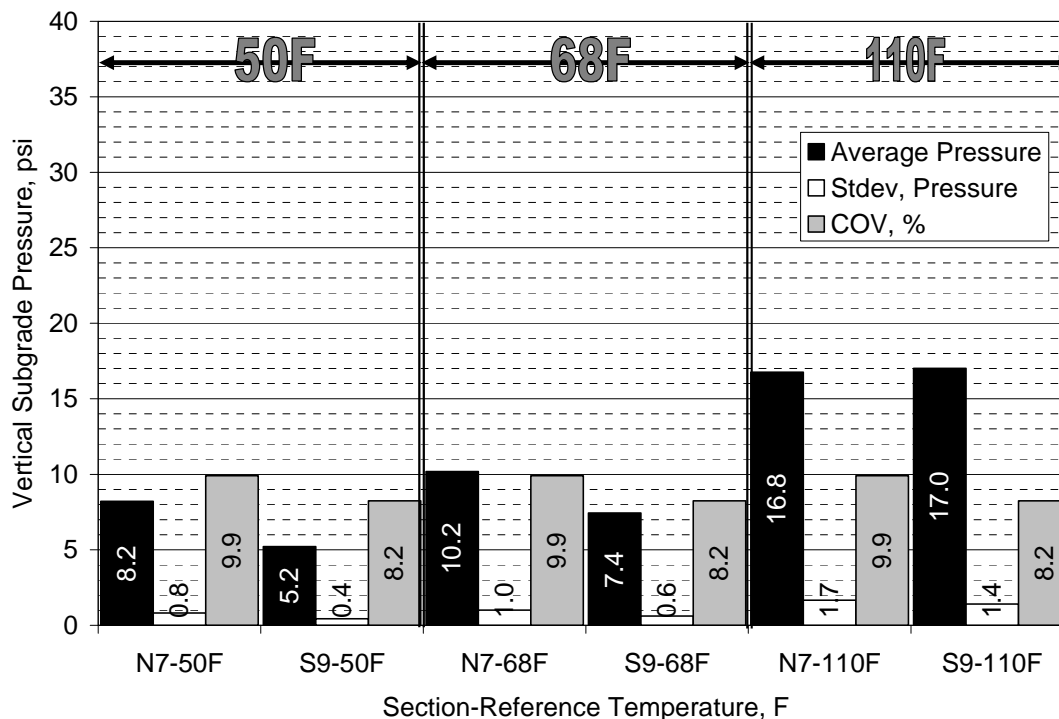
Figure 4.15 Subgrade Pressure Under Single Axles at Three Reference Temperatures

4.4 Pavement Response Over Time at 68F

Pavement responses normalized to 68°F were plotted against test date, as done with the backcalculated AC moduli data, to look for signs of distress or aging in the response measurements under single axles. It should again be noted that the regression coefficients from Table 4.1 were used for temperature normalization. In each graph, linear trendlines were determined for each data set so that the influence of pavement age could be evaluated. Within the strain plots, the data from N7 were plotted with and without the cutoff date.

Figure 4.16 clearly shows relatively consistent data for N7 through mid-April 2010 after which time the longitudinal strain measurements became very erratic. This phenomenon has already been discussed above, but is important to again recognize that the pavement reached a critical point at this time, likely due to gauge malfunction rather than pavement performance. The downward trend in N7, though in stark contrast to S9, is largely meaningless because of the high degree of scatter and relatively low R^2. The linear trendline for N7 through April 21, 2010 is more realistic and indicates no real change in strain over this short time period. Strain levels in S9 were unaffected by pavement age, as indicated by the trendline's flat slope and R^2 equal to 0.03.

Figure 4.17 also shows a general downward trend in N7's transverse strain response over time, with nearly 50% of the variability explained by pavement age when considering all the data. The effect was less dramatic, however, when considering the data only through April 21, 2010. The transverse strain in S9 was largely unaffected by age.

29
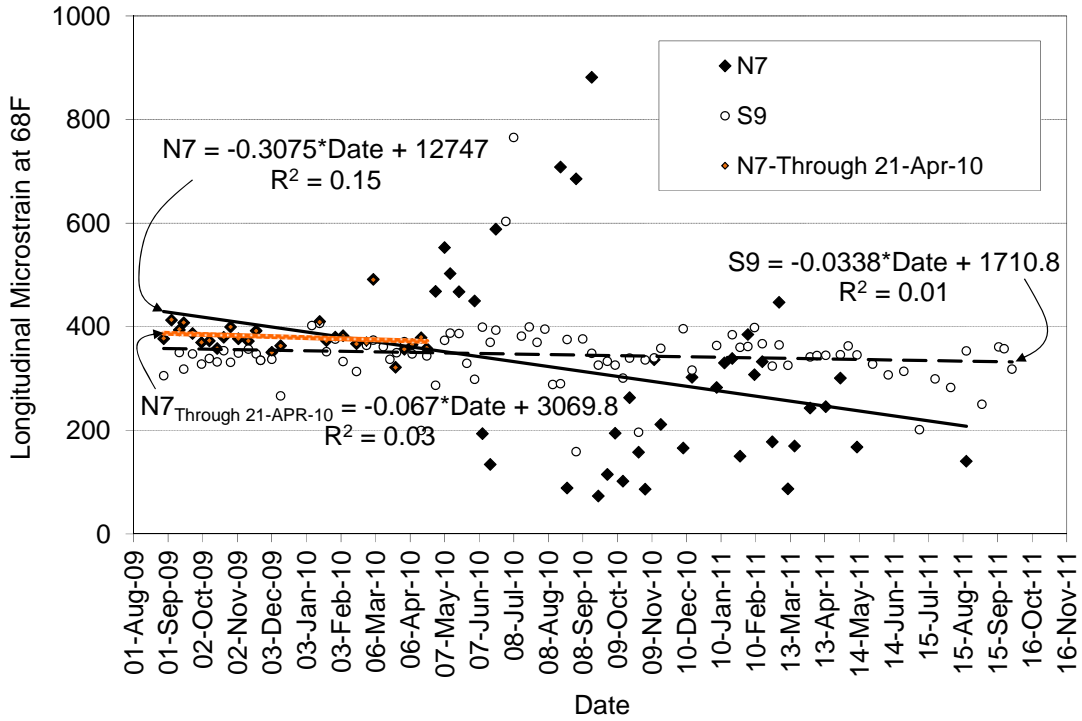
Figure 4.16 Longitudinal Microstrain Under Single Axles vs. Date at 68°F
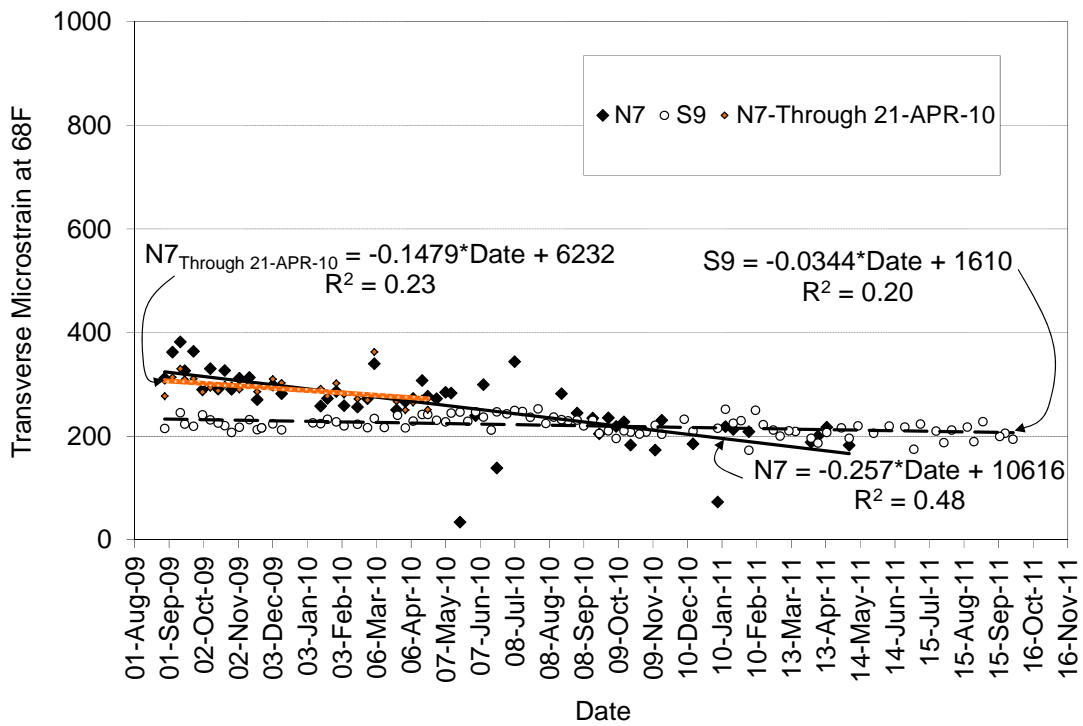
Figure 4.17 Transverse Microstrain Under Single Axles vs. Date at 68°F

Plots of pressure over time in Figures 4.18 and 4.19 show relatively stable pressure measurements in the base and subgrade layers, respectively. The generally low R^2 values (< 25%) combined with small slopes (< .006 psi per day reduction) lead to the reasonable conclusion that these measurements are affected, at this point, by what may be occurring in the AC layers.

The chart contains the following equations:

$N7 = -0.005 \cdot Date + 215.16$
$R^2 = 0.23$

$S9 = -0.0012 \cdot Date + 55.69$
$R^2 = 0.08$
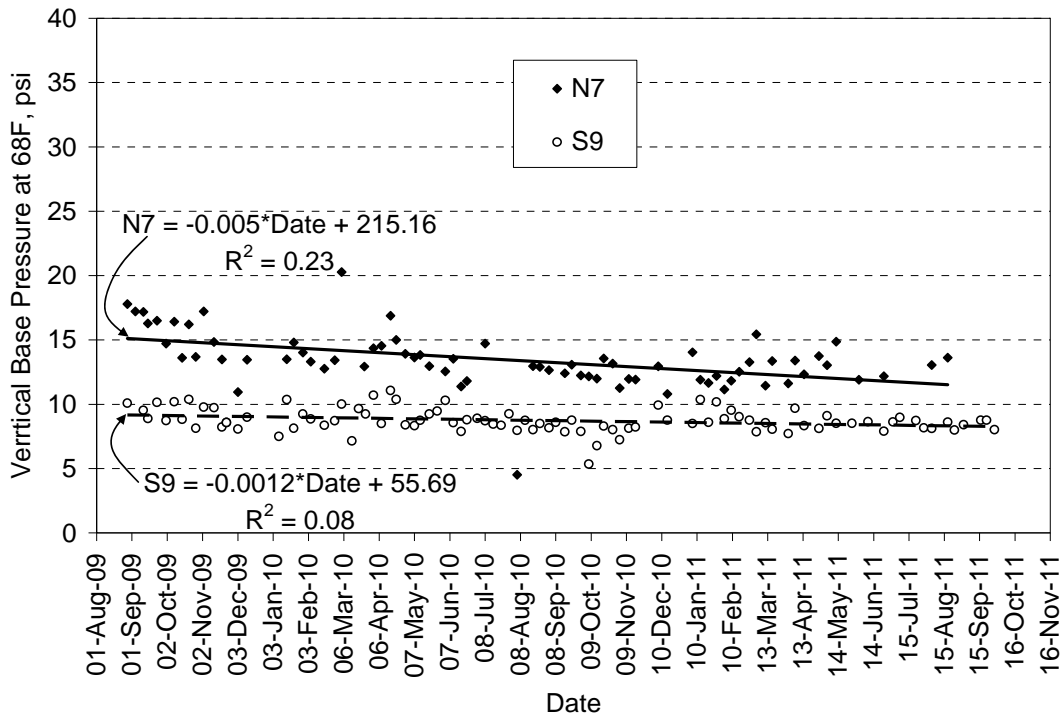
Figure 4.18 Base Pressure Under Single Axles vs. Date at 68°F
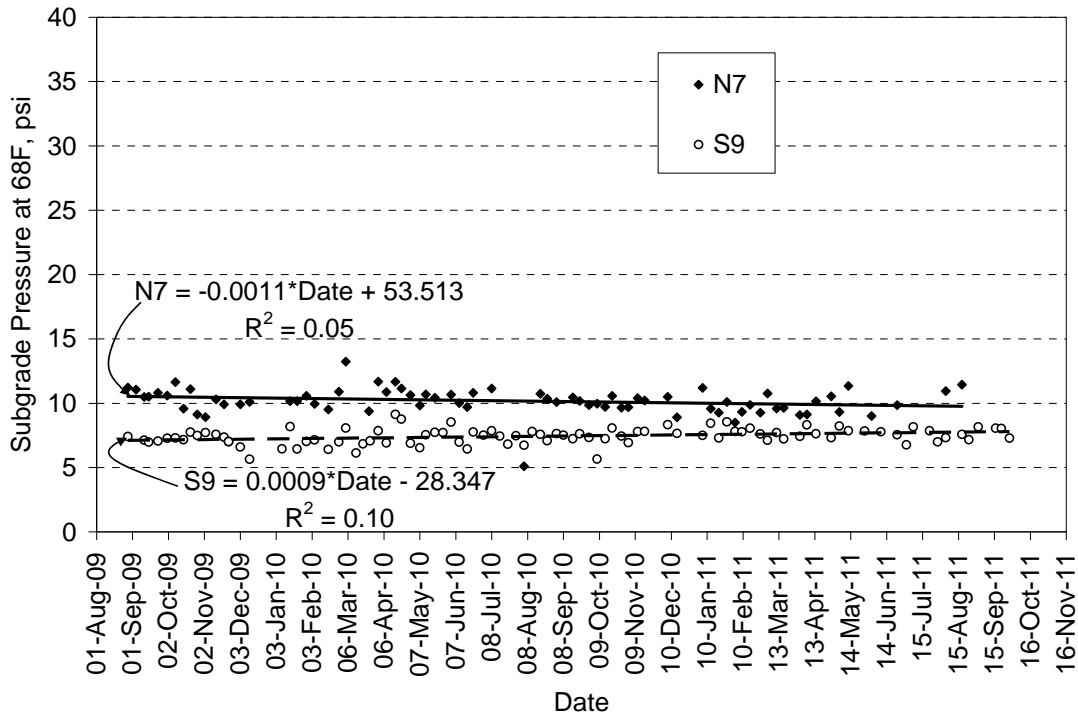
Figure 4.19 Subgrade Pressure Under Single Axles vs. Date at 68°F

5. PAVEMENT PERFORMANCE

At the conclusion of traffic, 10.14 million ESALs had been applied to the sections. At that time, there was no cracking evident on either of the sections. During the two-year test cycle, measurements of rutting and roughness (International Roughness Index (IRI)) were made using a Roadware ARAN van. Figure 5.1 illustrates the average rutting progression (both wheelpaths) in each section with a three-point moving average fit to each series, in addition to the accumulation of ESALs over time. As seen in previous research cycles (Timm et al., 2006; Willis et al., 2009), rutting tended to increase during summer months and level off during colder months. This was especially true during the first summer. However, the Kraton section did not appear to have increased rutting during subsequent summers and maintained rut depths less than 3 mm through the end of the experiment.

A statistical comparison of rutting between sections was conducted using final wire-line measurements made at the conclusion of traffic. Wire-line rutting measurement determines the rut depth from a straight line extending across the lane, parallel to the cross-slope, at the pavement surface and does not include any upward surface distortion that may be present. Using ten measurements per section, the average and standard deviation of rut depth in the outside (most severe) wheelpath were determined and plotted in Figure 5.2. Two-tailed t-tests (α=0.05) showed that the Kraton section was statistically lower than the control, though both were below the failure threshold of 12.5 mm (0.5 in.).
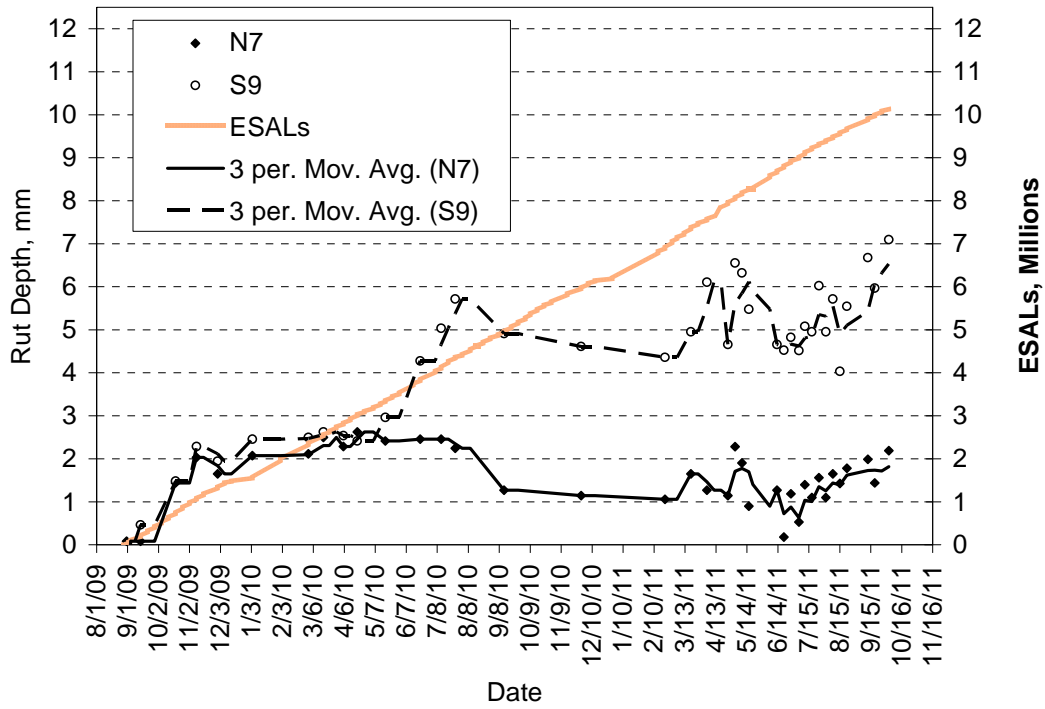
Figure 5.1 ARAN-Measured Rut Depths
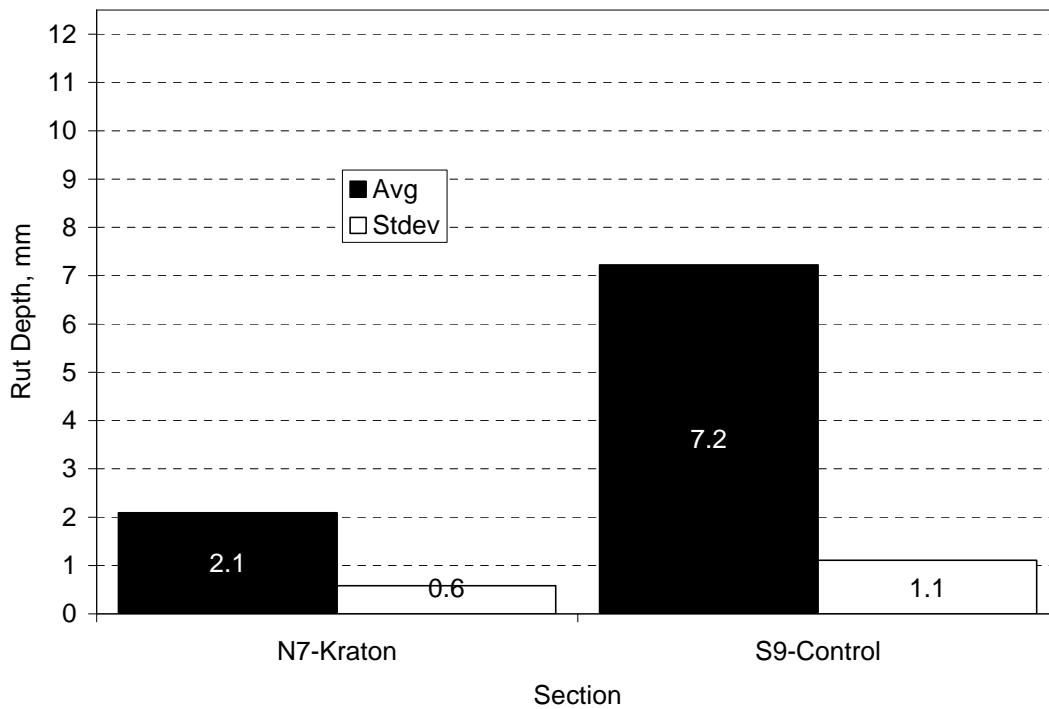
Figure 5.2 Final Wireline Rut Depths

Weekly ride quality measurements, quantified by the International Roughness Index (IRI), are shown in Figure 5.3 for each section with linear trendlines fit to each series. The control section clearly had very little change in IRI during the two-year period and was built considerably smoother than the Kraton section. Interestingly, although the Kraton section was built with greater roughness, it tended to become smoother over time. The roughness decreased by approximately 10 in./mile from start to finish. As documented in the earlier report (Timm et al., 2012), Figure 5.4 shows roughness versus distance in N7 at the start and end of the experiment subdivided into 25-ft. subsections. Clearly, the high IRI of N7 is driven by the first two segments, which have gotten smoother over time. Furthermore, at a maximum of 125 in./mile, the Kraton section was well below a commonly accepted threshold of 170 in./mile that would trigger some sort of rehabilitation. This 170 in./mile value, as reported by Shafizadeh and Mannering (2003), was recommended by the FHWA for "acceptable ride quality," in its 1998 National Strategic Plan for the National Highway System (NHS).
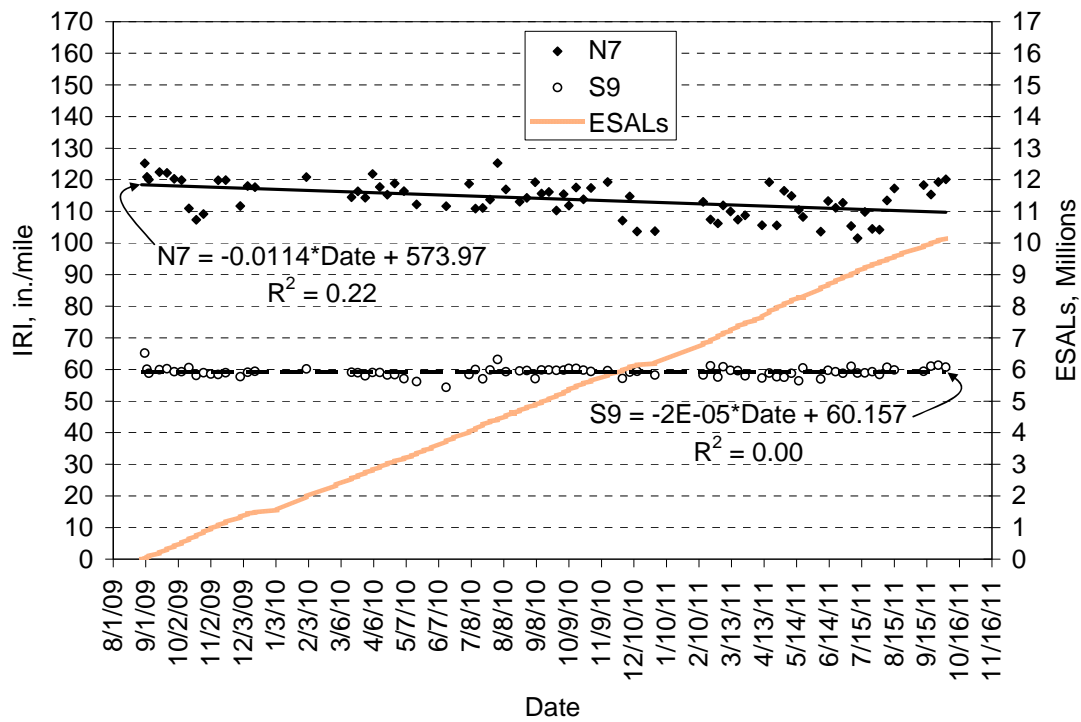
Figure 5.3 ARAN-Measured Pavement Roughness
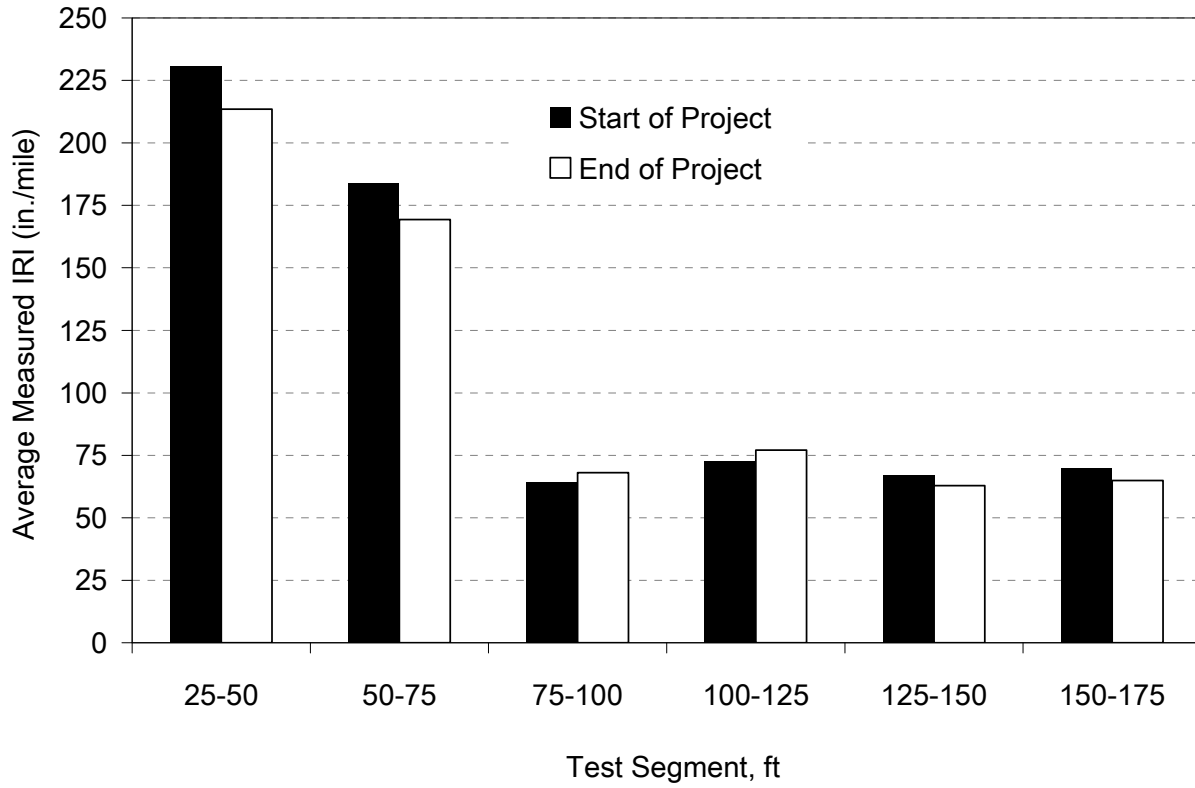
Figure 5.4 Roughness vs. Distance in Kraton Section (Timm et al., 2012)

6. KEY FINDINGS, CONCLUSIONS AND RECOMMENDATIONS
This report was intended to document additional lab testing and field performance of the Kraton and control sections under the full two-year, 10.14 million ESAL, research cycle at the NCAT Test Track. Based on the data presented herein the following key findings, conclusions and recommendations can be made:

6.1 Laboratory Characterization
1. S-VECD testing in the AMPT device showed that the Kraton base mixture was predicted to have a fatigue life more than one order of magnitude greater than the control mixture. These findings were in agreement with previous beam fatigue testing on these mixtures.
2. Based on results from HWTT, the Kraton base mixture had the largest SIP and, thus, was expected to have the most resistance to moisture damage. All four mixtures (Kraton base, Kraton surface, Control base and Control surface) had SIP values greater than commonly used thresholds.
3. While the HWTT rut depths were not statistically different for the four mixtures, the rutting rate of the control base mixture was statistically higher than those of the control surface and the Kraton mixtures. According to Texas total rut depth criteria, none of the tested mixtures were expected to have a rutting problem in the field.

6.2 Structural Response and Characterization
1. Differences in backcalculated layer moduli at three reference temperatures (50, 68 and 110°F) were found to be statistically significant. At the two lower temperatures, the control section had higher modulus while at 110°F, the Kraton section was higher. The increased modulus at high temperatures likely contributed to the improved rutting performance over the control section.
2. An examination of backcalculated composite AC modulus at 68°F data versus test date did not indicate the initial stages of bottom-up fatigue cracking in either of the test sections. Only minor, if any, aging effects were detected in the AC modulus data over time. It is recommended to leave the sections in place for further trafficking and FWD monitoring to evaluate over a longer time period.
3. Strong correlations between mid-depth pavement temperature and pavement response (AC strain, base pressure and subgrade pressure) were found for the control section. These strong correlations translated into relatively stable response measurements, normalized to 68°F, over time. This observation, combined with the normalized backcalculated AC modulus versus time, leads to the conclusion that the control section has not yet experienced cracking and/or significant aging.
4. The correlations between mid-depth pavement temperature and pavement response for the Kraton section were less strong that those observed in the control section. It appeared that April 21, 2010 could be used as a cut-off date between "stable" and "erratic" data. The erratic data appeared more related to gauge functionality than to pavement performance.
5. The measured response data demonstrated that the Kraton section experienced higher levels of stress and strain at low (50°F) and intermediate (68°F) temperatures. At the higher temperatures (110°F), the increased modulus appeared to generate equivalent strain levels for some, but not all, responses.
   a. Using data only prior to the cut-off date for the Kraton section, average longitudinal strain measurements normalized to 50 and 68°F were found statistically higher in the

Kraton section than the control. This was expected since the Kraton section was thinner and had lower moduli at these temperatures. However, at 110°F, the Kraton section had statistically equivalent average strain levels meaning the increased modulus overcame the thickness deficiency to generate similar strain levels.

b. Despite the Kraton section having statistically higher longitudinal strain at 68°F, the enhanced fatigue characteristics measured in the laboratory translated to an estimated 17 times improvement in expected fatigue life.

c. Average transverse strain levels in the Kraton section, using only data prior to April 21, 2010, were statistically higher than the control section at each of the three reference temperatures. This was expected due to the thickness advantage held by the control section. This was also the case for the vertical pressure measurements. An exception, however, was the vertical pressure in the subgrade at 110°F where the control and Kraton pressures were not statistically different.

6.3 Performance

1. At the conclusion of trafficking, neither section had experienced cracking. It is recommended that the sections be left in place for further trafficking and monitoring.

2. Rutting performance in the Kraton section was significantly better than the control section. However, both sections performed well with total rut depths less than 12.5 mm (0.5 in.)

3. The ride quality was significantly better in the control section than the Kraton section. However, neither section became rougher over time; the higher roughness in the Kraton section was attributed to as-built roughness not associated with the material itself.

REFERENCES

1. Allen, D.L. and R.C. Graves. Variability in Measurement of In-Situ Material Properties. *Proceedings, Fourth International Conference on the Bearing Capacity of Roads and Airfields*, Vol. 2, 1994, pp. 989-1005.

2. Anderson, R. M. *Asphalt Modification and Additives*. The Asphalt Handbook MS-4, 7th ed., Asphalt Institute, Lexington, 2007, pp. 86-89.

3. Brown, E.R., P.S. Kandhal, and J. Zhang. *Performance Testing for Hot Mix Asphalt*, Report 01-05, National Center for Asphalt Technology, Auburn University, November 2001.

4. Daniel, J.S, and Y. R. Kim. "Development of a Simplified Fatigue Test and Analysis Procedure Using a Viscoelastic, Continuum Damage Model." *Journal of Association of Asphalt Paving Technologists*, 2002.

5. Erkens, S. M. J. G. *Asphalt Concrete Response (ACRe), Determination, Modelling and Prediction*. Ph.D. Dissertation, Delft University of Technology, The Netherlands, 2002.

6. Halper, W. M, and G. Holden. Styrenic Thermoplastic Elastomers in Handbook of Thermoplastic Elastomers. 2nd ed., B. M. Walker and C. P. Rader, Eds., Van Nostrand Reinhold, New York, 1988.

7. Hou, T., B.S. Underwood, and Y.R. Kim. "Fatigue Performance Prediction of North Carolina Mixtures Using the Simplified Viscoelastic Contiuum Damage Model." *Journal of Association of Asphalt Paving Technologists*, 2010.

8. Kim, Y. R., M. Guddati, B. S. Underwood, T. Yun, V. Subramanian, and S. Savadatti. "Development of a Multiaxial Viscoelastoplastic Continuum Damage Model for Asphalt Mixtures." *Report No. FHWA-HRT-08-073*, FHWA, 2009.

9. Kim, Y. R., H.J. Lee, and D.N. Little. "Fatigue Characterization of Asphalt Concrete Using Viscoelasticity and Continuum Damage Theory." *Journal of Association of Asphalt Paving Technologists*, 1997: pp. 520-569.

10. Kluttz, R. Q., A. A. A. Molenaar, M. F. C.van de Ven, M.R. Poot, X. Liu, A. Scarpas and E.J. Scholten. Modified Base Courses for Reduced Pavement Thickness and Improved Longevity. *Proceedings of the International Conference on Perpetual Pavement*, October, 2009, Columbus, OH.

11. Molenaar, A.A.A., M.F.C. van de Ven, X. Liu, A. Scarpas, T.O. Medani and E.J. Scholten. Advanced Mechanical Testing of Polymer Modified Base Course Mixes. *Proceedings, Asphalt – Road for Life,* Copenhagen, May 2008, pp. 842-853.

12. Noureldin, A.S. Influence of Stress Levels and Seasonal Variations on In Situ Pavement Layer Properties. *Transportation Research Record No. 1448*, Washington, D.C., 1994, pp. 16-24.

13. Priest, A.L. and D.H. Timm. *Methodology and Calibration of Fatigue Transfer Functions for Mechanistic-Empirical Flexible Pavement Design*. Report No. 06-03, National Center for Asphalt Technology, Auburn University, 2006.

14. Scarpas, A. and J. Blaauwendraad. Experimental Calibration of a Constitutive Model for Asphaltic Concrete. *Proceedings of Euro-C Conference on the Computational Modelling of Concrete Structures*, Badgastein, Austria, April 1998.

15. Shafizadeh, K. and F. Mannering. Acceptability of Pavement Roughness on Urban Highways by Driving Public. *Transportation Research Record No. 1860*, Washington, D.C., 2003, pp. 187-193.

16. Taylor, A.J. and D.H. Timm. *Mechanistic Characterization of Resilient Moduli for Unbound Pavement Layer Materials*. Report No. 09-06, National Center for Asphalt Technology, Auburn University, 2009.

17. Timm, D.H., M.M. Robbins, J.R. Willis, N. Tran and A.J. Taylor. *Field and Laboratory Study of High-Polymer Mixtures at the NCAT Test Track*. Draft Report, National Center for Asphalt Technology, Auburn University, 2012.

18. Timm, D.H. *Design, Construction, and Instrumentation of the 2006 Test Track Structural Study*. Report No. 09-01, National Center for Asphalt Technology, Auburn University, 2009.

19. Timm, D.H. and A.L. Priest, "Wheel Wander at the NCAT Test Track," Report No. 05-02, National Center for Asphalt Technology, Auburn University, 2005.

20. Timm, D.H. and A.L. Priest, "Material Properties of the 2003 NCAT Test Track Structural Study," Report No. 06-01, National Center for Asphalt Technology, Auburn University, 2006.

21. Timm, D.H. and A.L. Priest. Flexible Pavement Fatigue Cracking and Measured Strain Response at the NCAT Test Track. *Proceedings of the 87th Annual Transportation Research Board*, Washington, D.C., 2008.

22. Timm, D.H., D.E. Newcomb and B. Birgisson. *Mechanistic-Empirical Flexible Pavement Thickness Design: The Minnesota Method*. Staff Paper, MN/RC-P99-10, Minnesota Department of Transportation, St. Paul, MN, 1999.

23. Underwood, B.S., Y.R. Kim, and M. Guddati. "Characterization and Performance Prediciton of ALF Mixtures Using a Viscoelastoplastic Contiuum Damage Model." *Journal of Association of Asphalt Paving Technologists*, 2006.

24. van de Ven, M.F.C., M.R. Poot and T.O. Medani. *Advanced Mechanical Testing of Polymer Modified Asphalt Mixtures.* Report 7-06-135-3, Road and Rail Engineering, Delft University of Technology, the Netherlands, April 2007.

25. von Quintus, H. *Quantification of the Effects of Polymer-Modified Asphalt*. Engineering Report ER 215, Asphalt Institute, 2005, pp. 1-8.

26. Willis, J.R. and D.H. Timm. *Field-Based Strain Thresholds for Flexible Perpetual Pavement Design*. Report No. 09-09, National Center for Asphalt Technology, Auburn University, 2009.

APPENDIX A – MIX DESIGN AND AS BUILT AC PROPERTIES

10/5/2009

Quadrant:	N
Section:	7 *Mix Type = Surface - Kraton*
Sublot:	1

Laboratory Diary

General Description of Mix and Materials

Design Method:	Super
Compactive Effort:	80 gyrations
Binder Performance Grade: *88-22*	
Modifier Type:	7.5% SBS
Aggregate Type:	Grn/Sand/Lms
Design Gradation Type:	Fine

Avg. Lab Properties of Plant Produced Mix

Sieve Size	Design	QC
25 mm (1"):	100	100
19 mm (3/4"):	100	100
12.5 mm (1/2"):	100	100
9.5 mm (3/8"):	100	100
4.75 mm (#4):	77	82
2.36 mm (#8):	60	63
1.18 mm (#16):	45	48
0.60 mm (#30):	31	32
0.30 mm (#50):	16	17
0.15 mm (#100):	9	10
0.075 mm (#200):	5.7	6.6
Binder Content (Pb):	5.9	6.3
Eff. Binder Content (Pbe):	5.3	5.7
Dust-to-Binder Ratio:	1.1	1.2
Rice Gravity (Gmm):	2.474	2.468
Avg. Bulk Gravity (Gmb):	2.375	2.367
Avg Air Voids (Va):	4.0	4.1
Agg. Bulk Gravity (Gsb):	2.667	2.678
Avg VMA:	16.2	17.2
Avg. VFA:	75	76

Construction Diary

Relevant Conditions for Construction

Completion Date:	July 22, 2009
24 Hour High Temperature (F):	88
24 Hour Low Temperature (F):	60
24 Hour Rainfall (in):	0.00
Planned Subot Lift Thickness (in):	1.3
Paving Machine:	Roadtec

Plant Configuration and Placement Details

Component	% Setting
Asphalt Content (Plant Setting)	6.2
89 Columbus Granite	36.0
8910 Opelika Limestone Screenings	23.0
M10 Columbus Granite	13.0
Shorter Coarse Sand	28.0

As-Built Sublot Lift Thickness (in):	1.1
Total Thickness of All 2009 Sublots (in):	5.8
Approx. Underlying HMA Thickness (in):	0.0
Type of Tack Coat Utilized:	NTSS-1HM
Target Tack Application Rate (gal/sy):	0.07
Approx. Avg. Temperature at Plant (F):	345
Avg. Measured Mat Compaction:	93.7%
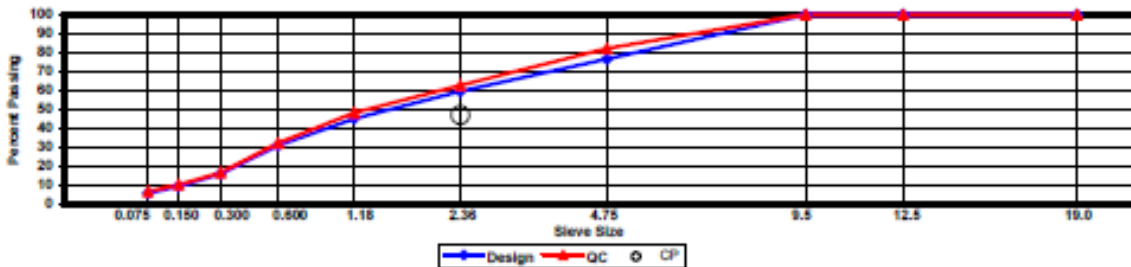
General Notes:
1) Mixes are referenced by quadrant (E=East, N=North, W=West, and S=South), section # (sequential) and sublot (top=1);
3) The total HMA thickness of all structural study sections (N1-N11 and S8-S12) ranges from 5-3/4 to 14 inches by design;
3) All non-structural sections are supprted by a uniform perpetual foundation in order to study surface mix performance;
4) SMA and OGFC refer to stone matrix asphalt and open-graded friction course, respectively; and
5) All liquid asphalt purchased for use in Track reconstruction contained LOF 6500 antistrip additive at a rate of 0.5 percent

10/5/2009

Quadrant:	N	
Section:	7	*Mix Type = Intermediate - Kraton*
Sublot:	2	

Laboratory Diary

General Description of Mix and Materials

Design Method:	Kraton
Compactive Effort:	80 gyrations
Binder Performance Grade: *88-22*	
Modifier Type:	7.5% SBS
Aggregate Type:	Lms/Sand/Gm
Design Gradation Type:	Fine

Avg. Lab Properties of Plant Produced Mix

Sieve Size	Design	QC
25 mm (1"):	100	98
19 mm (3/4"):	93	92
12.5 mm (1/2"):	82	82
9.5 mm (3/8"):	71	73
4.75 mm (#4):	52	56
2.36 mm (#8):	45	46
1.18 mm (#16):	35	37
0.60 mm (#30):	24	25
0.30 mm (#50):	12	13
0.15 mm (#100):	7	8
0.075 mm (#200):	3.9	5.2
Binder Content (Pb):	4.6	4.6
Eff. Binder Content (Pbe):	4.2	4.2
Dust-to-Binder Ratio:	0.9	1.2
Rice Gravity (Gmm):	2.570	2.549
Avg. Bulk Gravity (Gmb):	2.467	2.423
Avg Air Voids (Va):	4.0	4.9
Agg. Bulk Gravity (Gsb):	2.737	2.712
Avg VMA:	14.0	14.8
Avg. VFA:	72	67

Construction Diary

Relevant Conditions for Construction

Completion Date:	July 21, 2009
24 Hour High Temperature (F):	88
24 Hour Low Temperature (F):	60
24 Hour Rainfall (in):	0.00
Planned Subot Lift Thickness (in):	2.3
Paving Machine:	Roadtec

Plant Configuration and Placement Details

Component	% Setting
Asphalt Content (Plant Setting)	4.8
78 Opelika Limestone	30.0
57 Opelika Limestone	18.0
M10 Columbus Granite	25.0
Shorter Coarse Sand	27.0

As-Built Sublot Lift Thickness (in):	2.1
Total Thickness of All 2009 Sublots (in):	5.8
Approx. Underlying HMA Thickness (in):	0.0
Type of Tack Coat Utilized:	NTSS-1HM
Target Tack Application Rate (gal/sy):	0.07
Approx. Avg. Temperature at Plant (F):	345
Avg. Measured Mat Compaction:	92.7%
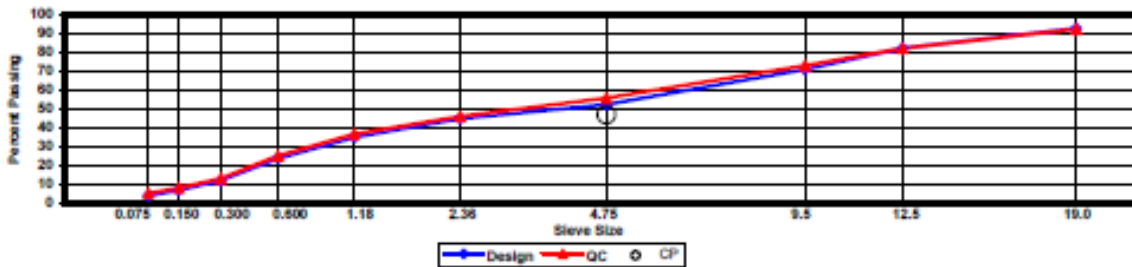
General Notes:
1) Mixes are referenced by quadrant (E=East, N=North, W=West, and S=South), section # (sequential) and sublot (top=1);
3) The total HMA thickness of all structural study sections (N1-N11 and S8-S12) ranges from 5-3/4 to 14 inches by design;
3) All non-structural sections are supprted by a uniform perpetual foundation in order to study surface mix performance;
4) SMA and OGFC refer to stone matrix asphalt and open-graded friction course, respectively; and
5) All liquid asphalt purchased for use in Track reconstruction contained LOF 6500 antistrip additive at a rate of 0.5 percent

10/5/2009

Quadrant:	N	
Section:	7	*Mix Type = Base - Kraton*
Sublot:	3	

Laboratory Diary

General Description of Mix and Materials

Design Method:		Kraton
Compactive Effort:		80 gyrations
Binder Performance Grade:	*88-22*	
Modifier Type:		7.5% SBS
Aggregate Type:		Lms/Sand/Grn
Design Gradation Type:		Fine

Avg. Lab Properties of Plant Produced Mix

Sieve Size	Design	QC
25 mm (1"):	100	98
19 mm (3/4"):	93	91
12.5 mm (1/2"):	82	81
9.5 mm (3/8"):	71	72
4.75 mm (#4):	52	55
2.36 mm (#8):	45	45
1.18 mm (#16):	35	36
0.60 mm (#30):	24	25
0.30 mm (#50):	12	12
0.15 mm (#100):	7	7
0.075 mm (#200):	3.9	4.6
Binder Content (Pb):	4.6	4.6
Eff. Binder Content (Pbe):	4.2	4.2
Dust-to-Binder Ratio:	0.9	1.1
Rice Gravity (Gmm):	2.570	2.545
Avg. Bulk Gravity (Gmb):	2.467	2.427
Avg Air Voids (Va):	4.0	4.6
Agg. Bulk Gravity (Gsb):	2.737	2.707
Avg VMA:	14.0	14.5
Avg. VFA:	72	68

Construction Diary

Relevant Conditions for Construction

Completion Date:	July 20, 2009
24 Hour High Temperature (F):	85
24 Hour Low Temperature (F):	60
24 Hour Rainfall (in):	0.00
Planned Subot Lift Thickness (in):	2.3
Paving Machine:	Roadtec

Plant Configuration and Placement Details

Component	% Setting
Asphalt Content (Plant Setting)	4.8
78 Opelika Limestone	30.0
57 Opelika Limestone	18.0
M10 Columbus Granite	25.0
Shorter Coarse Sand	27.0
As-Built Sublot Lift Thickness (in):	2.5
Total Thickness of All 2009 Sublots (in):	5.8
Approx. Underlying HMA Thickness (in):	0.0
Type of Tack Coat Utilized:	NA
Target Tack Application Rate (gal/sy):	NA
Approx. Avg. Temperature at Plant (F):	340
Avg. Measured Mat Compaction:	92.8%
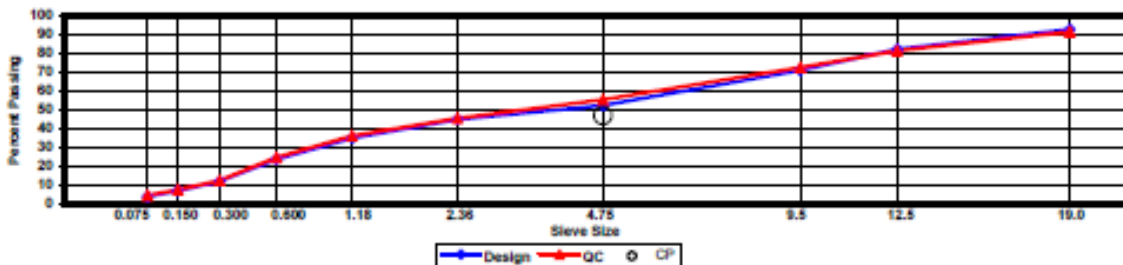
General Notes:
1) Mixes are referenced by quadrant (E=East, N=North, W=West, and S=South), section # (sequential) and sublot (top=1);
3) The total HMA thickness of all structural study sections (N1-N11 and S8-S12) ranges from 5-3/4 to 14 inches by design;
3) All non-structural sections are supprted by a uniform perpetual foundation in order to study surface mix performance;
4) SMA and OGFC refer to stone matrix asphalt and open-graded friction course, respectively; and
5) All liquid asphalt purchased for use in Track reconstruction contained LOF 6500 antistrip additive at a rate of 0.5 percent

10/5/2009

Quadrant: S
Section: 9   *Mix Type = Surface - Control*
Sublot: 1

Laboratory Diary			Construction Diary	
General Desccription of Mix and Materials			**Relevant Conditions for Construction**	

Design Method:		Super	Completion Date:	July 16, 2009
Compactive Effort:		80 gyrations	24 Hour High Temperature (F):	92
Binder Performance Grade:		76-22	24 Hour Low Temperature (F):	74
Modifier Type:		SBS	24 Hour Rainfall (in):	0.00
Aggregate Type:		Grn/Sand/Lms	Planned Subot Lift Thickness (in):	1.3
Design Gradation Type:		Fine	Paving Machine:	Roadtec

Avg. Lab Properties of Plant Produced Mix   **Plant Configuration and Placement Details**

Sieve Size	Design	QC	Component	% Setting
25 mm (1"):	100	100	Asphalt Content (Plant Setting)	6.5
19 mm (3/4"):	100	100		
12.5 mm (1/2"):	100	100	89 Columbus Granite	36.0
9.5 mm (3/8"):	100	100	8910 Opelika Limestone Screenings	23.0
4.75 mm (#4):	78	81	M10 Columbus Granite	13.0
2.36 mm (#8):	60	59	Shorter Coarse Sand	28.0
1.18 mm (#16):	46	46		
0.60 mm (#30):	31	31		
0.30 mm (#50):	16	16		
0.15 mm (#100):	10	9		
0.075 mm (#200):	5.8	6.0		
Binder Content (Pb):	5.8	6.1		
Eff. Binder Content (Pbe):	5.1	5.4		
Dust-to-Binder Ratio:	1.1	1.1		
			As-Built Sublot Lift Thickness (in):	1.2
Rice Gravity (Gmm):	2.483	2.472	Total Thickness of All 2009 Sublots (in):	7.0
Avg. Bulk Gravity (Gmb):	2.384	2.374	Approx. Underlying HMA Thickness (in):	0.0
Avg Air Voids (Va):	4.0	4.0	Type of Tack Coat Utilized:	NTSS-1HM
Agg. Bulk Gravity (Gsb):	2.667	2.670	Target Tack Application Rate (gal/sy):	0.04
Avg VMA:	15.8	16.5	Approx. Avg. Temperature at Plant (F):	335
Avg. VFA:	75	76	Avg. Measured Mat Compaction:	93.1%

General Notes:
1) Mixes are referenced by quadrant (E=East, N=North, W=West, and S=South), section # (sequential) and sublot (top=1);
3) The total HMA thickness of all structural study sections (N1-N11 and S8-S12) ranges from 5-3/4 to 14 inches by design;
3) All non-structural sections are supprted by a uniform perpetual foundation in order to study surface mix performance;
4) SMA and OGFC refer to stone matrix asphalt and open-graded friction course, respectively; and
5) All liquid asphalt purchased for use in Track reconstruction contained LOF 6500 antistrip additive at a rate of 0.5 percent

10/5/2009

Quadrant: S
Section: 9 *Mix Type = Intermediate - Control*
Sublot: 2

Laboratory Diary	Construction Diary

General Desscription of Mix and Materials

Design Method:	Super
Compactive Effort:	80 gyrations
Binder Performance Grade:	76-22
Modifier Type:	SBS
Aggregate Type:	Lms/Sand/Grn
Design Gradation Type:	Fine

Relevant Conditions for Construction

Completion Date:	July 14, 2009
24 Hour High Temperature (F):	93
24 Hour Low Temperature (F):	72
24 Hour Rainfall (in):	0.00
Planned Subot Lift Thickness (in):	2.8
Paving Machine:	Roadtec

Avg. Lab Properties of Plant Produced Mix

Sieve Size	Design	QC
25 mm (1"):	100	99
19 mm (3/4"):	93	92
12.5 mm (1/2"):	82	84
9.5 mm (3/8"):	71	76
4.75 mm (#4):	52	57
2.36 mm (#8):	45	47
1.18 mm (#16):	35	38
0.60 mm (#30):	24	26
0.30 mm (#50):	12	15
0.15 mm (#100):	7	9
0.075 mm (#200):	3.9	5.3
Binder Content (Pb):	4.7	4.4
Eff. Binder Content (Pbe):	4.1	3.9
Dust-to-Binder Ratio:	0.9	1.4
Rice Gravity (Gmm):	2.575	2.551
Avg. Bulk Gravity (Gmb):	2.472	2.439
Avg Air Voids (Va):	4.0	4.4
Agg. Bulk Gravity (Gsb):	2.737	2.695
Avg VMA:	13.9	13.5
Avg. VFA:	71	68

Plant Configuration and Placement Details

Component	% Setting
Asphalt Content (Plant Setting)	4.7
78 Opelika Limestone	30.0
57 Opelika Limestone	18.0
M10 Columbus Granite	25.0
Shorter Coarse Sand	27.0

As-Built Sublot Lift Thickness (in):	2.8
Total Thickness of All 2009 Sublots (in):	7.0
Approx. Underlying HMA Thickness (in):	0.0
Type of Tack Coat Utilized:	NTSS-1HM
Target Tack Application Rate (gal/sy):	0.07
Approx. Avg. Temperature at Plant (F):	335
Avg. Measured Mat Compaction:	92.8%
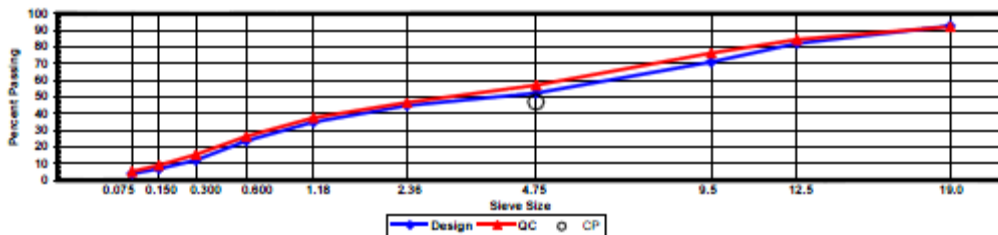
General Notes:
1) Mixes are referenced by quadrant (E=East, N=North, W=West, and S=South), section # (sequential) and sublot (top=1);
3) The total HMA thickness of all structural study sections (N1-N11 and S8-S12) ranges from 5-3/4 to 14 inches by design;
3) All non-structural sections are supprted by a uniform perpetual foundation in order to study surface mix performance;
4) SMA and OGFC refer to stone matrix asphalt and open-graded friction course, respectively; and
5) All liquid asphalt purchased for use in Track reconstruction contained LOF 6500 antistrip additive at a rate of 0.5 percent

45

10/5/2009

Quadrant: S
Section: 9   *Mix Type = Base - Control*
Sublot: 3

Laboratory Diary			Construction Diary	

General Desscription of Mix and Materials

Design Method:	Super
Compactive Effort:	80 gyrations
Binder Performance Grade:	67-22
Modifier Type:	NA
Aggregate Type:	Lms/Sand/Grn
Design Gradation Type:	Fine

Relevant Conditions for Construction

Completion Date:	July 3, 2009
24 Hour High Temperature (F):	92
24 Hour Low Temperature (F):	69
24 Hour Rainfall (in):	0.00
Planned Subot Lift Thickness (in):	3.0
Paving Machine:	Roadtec

Avg. Lab Properties of Plant Produced Mix

Sieve Size	Design	QC
25 mm (1"):	100	99
19 mm (3/4"):	93	95
12.5 mm (1/2"):	84	87
9.5 mm (3/8"):	73	77
4.75 mm (#4):	55	56
2.36 mm (#8):	47	46
1.18 mm (#16):	36	37
0.60 mm (#30):	25	26
0.30 mm (#50):	14	15
0.15 mm (#100):	8	9
0.075 mm (#200):	4.6	5.1
Binder Content (Pb):	4.6	4.7
Eff. Binder Content (Pbe):	4.1	4.2
Dust-to-Binder Ratio:	1.1	1.2
Rice Gravity (Gmm):	2.574	2.540
Avg. Bulk Gravity (Gmb):	2.471	2.439
Avg Air Voids (Va):	4.0	4.0
Agg. Bulk Gravity (Gsb):	2.738	2.699
Avg VMA:	13.9	13.9
Avg. VFA:	71	71

Plant Configuration and Placement Details

Component	% Setting
Asphalt Content (Plant Setting)	4.9
78 Opelika Limestone	30.0
57 Opelika Limestone	18.0
M10 Columbus Granite	25.0
Shorter Coarse Sand	27.0

As-Built Sublot Lift Thickness (in):	3.0
Total Thickness of All 2009 Sublots (in):	7.0
Approx. Underlying HMA Thickness (in):	0.0
Type of Tack Coat Utilized:	NA
Target Tack Application Rate (gal/sy):	NA
Approx. Avg. Temperature at Plant (F):	325
Avg. Measured Mat Compaction:	92.6%

General Notes:
1) Mixes are referenced by quadrant (E=East, N=North, W=West, and S=South), section # (sequential) and sublot (top=1);
3) The total HMA thickness of all structural study sections (N1-N11 and S8-S12) ranges from 5-3/4 to 14 inches by design;
3) All non-structural sections are supprted by a uniform perpetual foundation in order to study surface mix performance;
4) SMA and OGFC refer to stone matrix asphalt and open-graded friction course, respectively; and
5) All liquid asphalt purchased for use in Track reconstruction contained LOF 6500 antistrip additive at a rate of 0.5 percent